Protein phosphatase 2A B55β limits CD8⁺ T cell lifespan following cytokine withdrawal

Noé Rodríguez-Rodríguez,[1,2,3] Iris K. Madera-Salcedo,[1] J. Alejandro Cisneros-Segura,[1] H. Benjamín García-González,[1] Sokratis A. Apostolidis,[3] Abril Saint-Martin,[1] Marcela Esquivel-Velázquez,[1] Tran Nguyen,[3] Dámaris P. Romero-Rodríguez,[4] George C. Tsokos,[3] Jorge Alcocer-Varela,[1] Florencia Rosetti,[1] and José C. Crispín[1,5]

[1]Departamento de Inmunología y Reumatología, Instituto Nacional de Ciencias Médicas y Nutrición Salvador Zubirán, Mexico City, Mexico. [2]Departamento de Inmunología, Instituto de Investigaciones Biomédicas, Universidad Nacional Autónoma de México (UNAM), Mexico City, Mexico. [3]Division of Rheumatology, Beth Israel Deaconess Medical Center and Harvard Medical School, Boston, Massachusetts, USA. [4]Flow Cytometry Core Facility, Instituto Nacional de Enfermedades Respiratorias "Ismael Cosío Villegas", Mexico City, Mexico. [5]Tecnologico de Monterrey, Escuela de Medicina y Ciencias de la Salud, Monterrey, Mexico.

How T cells integrate environmental cues into signals that limit the magnitude and length of immune responses is poorly understood. Here, we provide data that demonstrate that B55β, a regulatory subunit of protein phosphatase 2A, represents a molecular link between cytokine concentration and apoptosis in activated CD8⁺ T cells. Through the modulation of AKT, B55β induced the expression of the proapoptotic molecule Hrk in response to cytokine withdrawal. Accordingly, B55β and Hrk were both required for in vivo and in vitro contraction of activated CD8⁺ lymphocytes. We show that this process plays a role during clonal contraction, establishment of immune memory, and preservation of peripheral tolerance. This regulatory pathway may represent an unexplored opportunity to end unwanted immune responses or to promote immune memory.

Protein phosphatase 2A (PP2A) is a serine/threonine phosphatase that regulates a large number of cellular processes, including apoptosis (1). PP2A is ubiquitously expressed, and defects in its activity and/or expression have been linked to cancer (2), neurodegenerative diseases (3), and autoimmunity (4). PP2A, as other serine/threonine phosphatases, is comprised of 3 subunits: scaffold (PP2A A), catalytic (PP2A C), and regulatory (PP2A B) (5). The scaffold and catalytic subunits assemble into a heterodimer that can associate in a mutually exclusive manner to a relatively large number of regulatory subunits. The choice of regulatory subunit determines, to a large extent, the subcellular location and target specificity of the holoenzyme (5).

Altered expression and activity of PP2A C in T cells have been documented in patients with systemic lupus erythematosus (SLE), a chronic autoimmune disease (4). In mice, increased expression of PP2A C in T cells promoted immune-mediated glomerulonephritis (6), whereas Treg-specific PP2A A deficiency annulled Treg suppressive function and caused early onset systemic autoimmunity (7). Thus, the correct function of PP2A is of utmost importance for T cell function.

Indirect evidence suggests that the B55β regulatory subunit of PP2A controls death and survival in different cell lineages. Expansion of a CAG repeat in the 5′ region of *PPP2R2B*, the gene that encodes B55β, causes type 12 spinocerebellar ataxia (8). The pathogenic repeat has been proposed to increase the expression of B55β (9) and cause disease by facilitating neuronal death (10, 11). On the other hand, decreased B55β expression, caused by promoter hypermethylation, has been linked to several types of cancer (12–14). In patients with SLE, defective expression of B55β in activated T cells is associated with resistance to apoptosis (15, 16). Therefore, although little is known about the function(s) of B55β in normal cell physiology, data produced in different experimental and clinical settings indicate that its expression facilitates cell death whereas its absence may allow abnormal cell survival and transformation.

Apoptosis represents the main mechanism responsible for the elimination of activated T cell clones during immune responses (17). Accordingly, defects in molecules that regulate the extrinsic and intrinsic pathways of apoptosis result in immune responses of excessive magnitude or length (18). During acute immune responses, T cell survival relies on environmental cues, including antigen and cytokine concentrations, but how these extrinsic elements or their absence trigger apoptosis is unknown. Here, we identify B55β as an essential molecule that controls T cell survival during the termination of immune responses and show that in human and mouse cells it regulates apoptosis through a conserved pathway that culminates in the induction of the proapoptotic molecule Hrk.

Results

B55β controls the lifespan of activated CD8⁺ T cells. Defective expression of the B55β regulatory subunit of PP2A is associated with resistance to cytokine withdrawal–induced death (CWID) in activated T cells from patients with SLE (15). To determine the role of B55β in the immune response, and in particular to define its participation in the regulation of apoptosis of activated T cells, we used a *Ppp2r2b* conditional knockout (cKO) mouse from the trans-NIH Knock-Out Mouse Project (KOMP) reposi-

Authorship note: NRR and IKMS are co–first authors.
Conflict of interest: The authors have declared that no conflict of interest exists.

Submitted: April 10, 2019; **Accepted:** July 31, 2020; **Published:** October 12, 2020.
Reference information: *J Clin Invest*. 2020;130(11):5989–6004.
https://doi.org/10.1172/JCI129479.

tory to generate a T cell–specific B55β cKO in the B6 background (*Ppp2r2b*$^{fl/fl}$ *Cd4*.Cre^{+}).

T cell–specific B55β deficiency did not affect T cell ontogeny or thymocyte populations and peripheral T cell subsets were numerically normal in 6-week-old cKO mice (Supplemental Figure 1A; supplemental material available online with this article; https://doi.org/10.1172/JCI129479DS1). However, as cKO mice aged, they exhibited a gradual decrease in the frequency of naive (CD44^{-}CD62L^{+}) T cells and a reciprocal increase in CD44^{+}CD62L^{+} central memory (CM) T cells. No consistent differences in the abundance of CD44^{+}CD62L^{-} effector memory (EM) T cells were observed (Supplemental Figures 2 and 3). The accumulation of CM T cells was mainly due to the presence of increased numbers of CM CD8^{+} T cells. Interestingly, aged mice accumulated a large amount of IFN-γ–producing CD8^{+} (WT 24.9 ± 1.6 vs. cKO 39.1 ± 3.4, P = 0.003) and CD4^{+} (WT 3.7 ± 0.4 vs. cKO 6.2 ± 0.6, P = 0.005) T cells (Supplemental Figure 3).

To define the role of B55β during an immune response, we generated B55β-deficient OT-I mice (*Ppp2r2b*$^{fl/fl}$ *Cd4*.Cre^{+} OT-I). We isolated CD8^{+} T cells from OT-I cKO and WT (*Ppp2r2b*$^{+/+}$ *Cd4*.Cre^{+} OT-I) mice, adoptively transferred them into CD45.1^{+} recipients, and infected them with ovalbumin-expressing recombinant *Listeria monocytogenes* (LM-OVA). At day 2, there were no differences in the number of CFU of *L. monocytogenes* isolated from the livers of mice that had received WT and cKO cells (WT 585 ± 235 vs. cKO 358 ± 111, P = 0.415), suggesting that deficiency of B55β does not affect the effector function of CD8^{+} T cells. At day 7, numbers of WT and cKO OT-I cells were similar, suggesting that B55β deficiency does not affect CD8^{+} T cell expansion (Figure 1A). To confirm this, we adoptively transferred CD45.1/2 WT and CD45.2 cKO OT-I cells, in a 1:1 ratio, into CD45.1 recipient mice and infected them with LM-OVA. At day 4 after infection (p.i.) EdU incorporation confirmed that antigen-induced proliferation is not affected by absence of B55β (Supplemental Figure 4). In contrast to what was observed during clonal expansion, the number of cKO cells was significantly higher during the contraction phase of the immune response. OT-I cKO cells were 2-fold more abundant at day 14 (1.29 ± 0.11 M vs. 2.76 ± 0.10 M, P = 0.0003) and 5-fold more abundant at day 30 (0.4 ± 0.11 M vs. 2.0 ± 0.30 M, P = 0.0008) p.i. than the number of WT OT-I cells (Figure 1A).

B55β deficiency did not alter the distribution of naive and activated/memory CD8^{+} T cells during the acute infection. As shown in Figure 1B, naive OT-I T cells virtually disappeared by day 7 p.i. and were replaced mostly by EM cells. The frequency of the latter ebbed and, at day 30, CM cells represented the most abundant OT-I cell subset in the spleens of infected mice.

Absence of B55β caused an accumulation of EM and CM cells, but the effect was more marked in CM cells (Figure 1C). This was not explained by different kinetics, because the contraction slope of WT EM and CM cells was similar (EM –3.6 vs. CM –3.3) (Supplemental Figure 5A). When WT OT-I cells were adoptively transferred, only 12.7% and 3.2% of the EM cells present at day 7 p.i. were found at days 14 and 30, respectively. Deficiency of B55β significantly increased the number of EM cells at day 14 (26.6%, P = 0.001) and day 30 (11.3%, P = 0.001), but the contraction slope was still steep (Figure 1C and Supplemental Figure 5B). The fraction of WT CM T cells found at days 14 and 30 p.i. was 42.1% and 15.6%, respectively. In the case of cKO OT-I cells, the number of CM cells found at days 14 and 30 p.i. was not different than the number of CM cells found at the peak of the response (day 7) when considered as absolute (day 14: 1.3 ± 0.1 M vs. 1.15 ± 0.1 M, P = 0.19; day 30: 1.3 ± 0.1 M vs. 1.27 ± 0.6 M, P = 0.91) or relative (day 14: 100% vs. 88.5%; day 30: 100% vs. 97.9%) numbers (Figure 1C). Accordingly, contraction of cKO CM OT-I cells was negligible (slope 0.03) and markedly different from the kinetics of WT CM cells (day 14 P = 0.004; day 30 P = 0.001) (Figure 1C and Supplemental Figure 5).

Analysis of expression of CD127 (IL-7Rα) and killer cell lectin-like receptor subfamily G member 1 (KLGR1) in WT and cKO OT-I T cells showed that at day 7 p.i. there were no differences in the abundance of CD127^{+} KLRG1^{-} memory precursor cells or CD127^{-} KLRG1^{+} short-lived effector cells (Figure 1D). However, at days 14 and 30, the numbers of both populations were significantly higher within B55β-deficient cKO OT-I cells (Figure 1E).

We quantified IFN-γ–producing capacity in WT and cKO OT-I cells upon ex vivo restimulation with their cognate antigen, an OVA-derived peptide (SIINFEKL). As shown in Figure 1, F and G, at day 7 the percentage (as well as the absolute number) of cells able to produce IFN-γ was similar in WT and cKO OT-I cells. However, at days 14 and 30, a higher percentage of cKO cells were IFN-γ^{+} (Figure 1G) and these differences were reflected in approximately 3-fold (0.39 ± 0.06 M vs. 1.28 ± 0.09 M, P = 0.0004) and approximately 9-fold (0.1 ± 0.04 M vs. 0.98 ± 0.18 M, P = 0.0007) increases in splenic IFN-γ–producing OT-I cells at days 14 and 30, respectively, within cKO OT-I cells when compared with their WT counterparts (Figure 1F).

Collectively, these results suggest that B55β regulates the lifespan of activated CD8^{+} T cells, in particular of CM CD8^{+} T cells. This role is exerted during steady state and at the resolution of an acute immune response triggered by an intracellular bacterium. Moreover, these results indicate that the accumulation of activated CD8^{+} T cells caused by the absence of B55β is not caused by an immune response of increased magnitude or by prolonged antigen persistence, but probably to decreased clonal contraction.

B55β is necessary for cytokine withdrawal–induced apoptosis. Our results, along with previously published work that associated defective B55β expression with resistance to CWID (15, 16), compelled us to analyze whether increased survival of activated CD8^{+} T cells was caused by defective apoptosis. To this end, we quantified apoptosis in adoptively transferred WT and cKO OT-I cells 30 days after infection with LM-OVA. As shown in Figure 2, A and B, the percentage of OT-I cells that exhibited apoptotic features was significantly decreased in cKO cells as compared with their WT counterparts (WT 18.7% ± 3.8% vs. cKO 6.7% ± 1.3%, P = 0.033). In concordance, caspase-3 activation was significantly lower in OT-I T cells deficient in B55β (WT 7.4% ± 0.8% vs. cKO 5.6% ± 0.4%, P = 0.032) when assessed 14 days after infection with LM-OVA (Figure 2C).

Clearance of activated T cells at the termination of acute immune responses is a complex process in which several molecules that regulate the mitochondrial pathway of apoptosis have been involved (19, 20). Loss of antigen, regulatory T (Treg) cell function, and cytokine withdrawal are considered key elements that trigger the demise of activated T cells (18). To determine

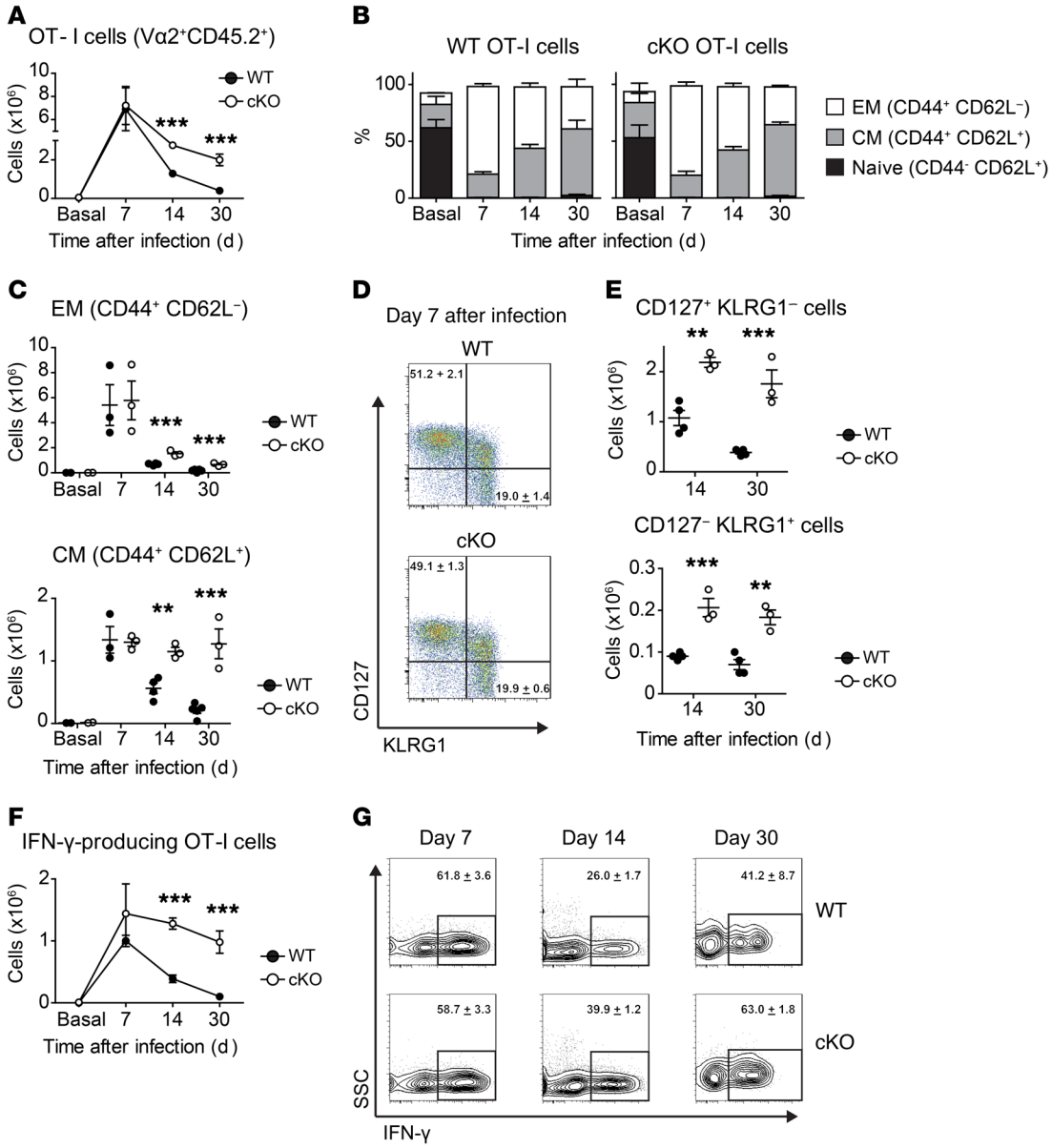

Figure 1. B55β regulates survival of activated T cells. A quantity of 10^6 OT-I CD45.2$^+$ *Ppp2r2b*$^{+/+}$ *Cd4*.Cre$^+$ (WT) or *Ppp2r2b*$^{fl/fl}$ *Cd4*.Cre$^+$ (cKO) cells were adoptively transferred into WT CD45.1$^+$ mice. The next day, 10^4 CFU of ovalbumin-expressing *Listeria monocytogenes* (LM-OVA) were i.v. injected into the recipient mice. (**A**) OT-I cells (CD45.2$^+$ CD8$^+$ Vα2$^+$ Vβ5$^+$) quantified in the spleens of recipient mice before infection (Basal) and at the indicated time points. (**B**) Frequency of naive (CD44$^-$ CD62L$^+$), EM (CD44$^+$ CD62L$^-$), and CM (CD44$^+$ CD62L$^+$) cells within donor-derived OT-I cells. (**C**) OT-I EM and CM cell numbers in spleens of recipient mice are quantified at the indicated time points. Each symbol represents a mouse. Mean and SEM are indicated by horizontal lines. (**D**) Representative dot plots of CD127 (IL-7Rα) and KLGR1 expression on adoptively transferred OT-I cells at day 7 after infection with LM-OVA. Numbers in the dot plots represent the mean ± SEM of the indicated populations. (**E**) Absolute numbers of OT-I CD127$^+$ KLGR1$^-$ and CD127$^-$ KLGR1$^+$ cells in spleens of recipient mice. (**F**) Spleen cells from infected mice, stimulated ex vivo with SIINFEKL, in the presence of Brefeldin A. Results are expressed as absolute numbers of IFN-γ–producing OT-I T cells (mean ± SEM). (**G**) Representative contour plots from spleen cells stimulated with SIINFEKL (gated in CD45.2$^+$ CD8$^+$ Vα2$^+$ Vβ5$^+$ donor-derived OT-I cells). Numbers represent mean ± SEM of the IFN-γ$^+$ populations. Results from 1 representative of 3 experiments (n = 3–5 mice/group) are shown (**A**–**G**). For comparison of the means, unpaired 2-tailed t tests were used in **A**, **C**, **E**, and **F**; $^{**}P \le 0.01$, $^{***}P \le 0.001$.

whether B55β deficiency impairs CWID, we activated polyclonal T cells from WT or cKO mice in vitro with anti-CD3 and anti-CD28 and expanded them in the presence of IL-2. After 10 days, cells were replated in fresh full RPMI devoid of IL-2, in the presence of a neutralizing anti–IL-2 antibody, to induce CWID (21). Induction of apoptosis was significantly decreased in B55β-deficient T cells (WT 36.7% ± 1.0% vs. cKO 25.6% ± 1.5%, $P < 0.001$) (Figure 2, D and E). As in the in vivo setting, the consequences of B55β absence were more marked in CD8$^+$ (WT 23.7% ± 0.6% vs. cKO 15.4% ± 1.3%, $P < 0.001$), than in CD4$^+$ T cells (WT 14.6% ± 1.1% vs. cKO 9.4% ± 1.2%, $P < 0.05$). Because FoxP3$^+$ Treg cells contribute, through IL-2 deprivation, to CD8$^+$ clonal contraction (22), we analyzed whether B55β deficiency could also affect Treg cell kinetics during LM-OVA infection. We observed a modest, albeit statistically significant, increment in Treg cell frequency in mice at days 7 and 30 following infection with LM-OVA in B55β cKO

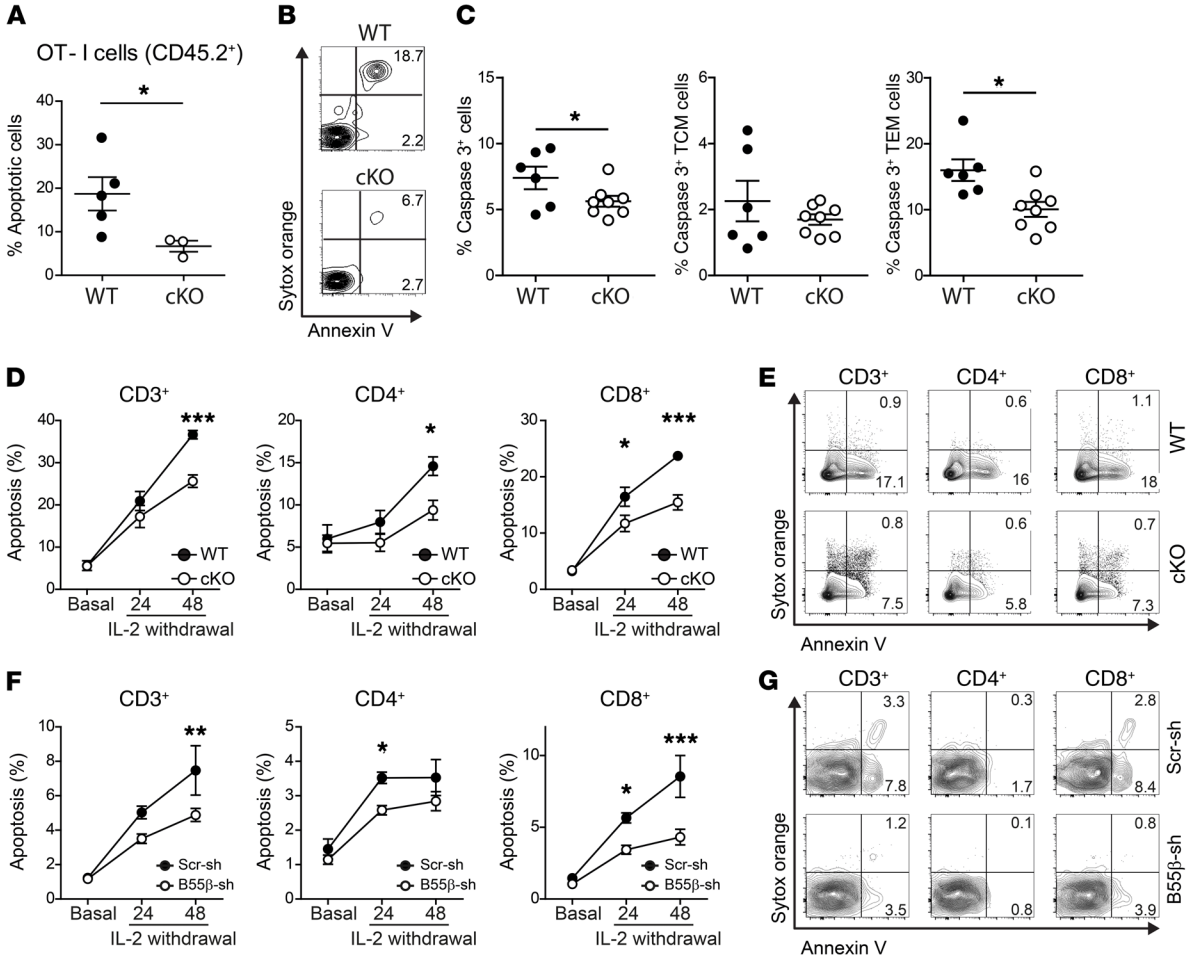

Figure 2. B55β is necessary for CWID. (**A**–**C**) OT-I CD45.2$^+$ *Ppp2r2b*$^{+/+}$ (WT) or *Ppp2r2b*$^{fl/fl}$ (cKO) cells were adoptively transferred into CD45.1$^+$ mice. The next day, LM-OVA was injected. After 30 days (**A** and **B**) or 14 days (**C**), the percentage of apoptotic OT-I cells (CD45.2$^+$ CD8$^+$ Vα2$^+$ Vβ5$^+$) was quantified as Annexin V binding (**A** and **B**) or caspase-3 activation (**C**) in spleens. Cumulative data from 2 experiments (n = 3–8 mice/group) are shown in **A** and **C**. $^*P \le 0.05$, unpaired 2-tailed t test. Representative contour plots of OT-I cells (**B**). Numbers represent mean of the indicated populations. (**D** and **E**) T cells from *Ppp2r2b*$^{+/+}$ *Cd4*.Cre$^+$ (WT) or *Ppp2r2b*$^{fl/fl}$ *Cd4*.Cre$^+$ (cKO) mice were stimulated in vitro with anti-CD3 and anti-CD28 (2 μg/mL). Fresh RPMI and IL-2 (100 U/mL) were replenished every 48 hours. At day 10, cells were counted and resuspended in fresh RPMI (10^6 cells per mL) devoid of IL-2, in the presence of a neutralizing anti–IL-2 antibody (5 μg/mL). Apoptosis was quantified before (basal) and after 24 and 48 hours of cytokine withdrawal. Results are presented as mean ± SEM. Cumulative results from 3 independent experiments (n = 2–4 mice/group/experiment) are shown. $^*P \le 0.05$, $^{***}P \le 0.001$ (2-way ANOVA with Bonferroni's posttest). Representative contour plots of WT and cKO cells, 48 hours after IL-2 withdrawal (**E**). (**F**) Human T cells were activated and infected in vitro as detailed in Supplemental Figure 7. Apoptosis was quantified after IL-2 withdrawal in lentiviral-infected cells (mCherry$^+$) at the indicated time points. Results are presented as mean ± SEM. Cumulative results from 4 experiments (n = 1/experiment). $^*P \le 0.05$, $^{**}P \le 0.01$, $^{***}P \le 0.001$ (2-way ANOVA with Bonferroni's posttest). (**G**) Representative contour plots at 48 hours after IL-2 deprivation.

mice. No differences in absolute Treg cell numbers were observed, suggesting that increased Treg cell frequency represents a compensatory mechanism triggered by failed CD8$^+$ clonal contraction (Supplemental Figure 6).

We generated lentiviral particles encoding short hairpin RNAs (shRNA) to silence the expression of B55β (*PPP2R2B*) in human T cells. T cells from healthy subjects were activated in vitro with OKT3 and anti-CD28 and infected with lentiviruses encoding B55β-specific (B55β-sh) or a scrambled control shRNA (Scr-sh) (Supplemental Figure 7). After 10 days of expansion, T cells were deprived of IL-2 and apoptosis was quantified in effectively infected (mCherry$^+$) cells. As shown in Figure 2, F and G, B55β silencing in human T cells significantly decreased apoptosis in total T cells (Scr-sh 7.5% ± 1.4% vs. B55β-sh 4.9% ± 0.4%, $P < 0.01$), CD4$^+$ T cells (Scr-sh 3.5% ± 0.2% vs. B55β-sh 2.6% ± 0.1%, $P < 0.05$), and CD8$^+$ T cells (Scr-sh 8.5% ± 1.5% vs. B55β-sh 4.3% ± 0.5%, $P < 0.001$). These results indicate that B55β is necessary for human and mouse T cells to undergo apoptosis in response to cytokine withdrawal and suggest that the accumulation of activated CD8$^+$ T cells in the B55β-deficient animal is due to the abnormal survival of activated clones.

IL-2 withdrawal induces AKT dephosphorylation in a B55β-dependent manner. The AKT/mTOR signaling pathway is an ancient system that allows cells to adapt to changes in their environment, in particular fluctuations in nutrients and growth factors (23). PP2A regulates the activity of the AKT/mTOR pathway at different levels (24) and in many cell lineages, including T cells (7). Because CWID represents a cellular response to a decline in the

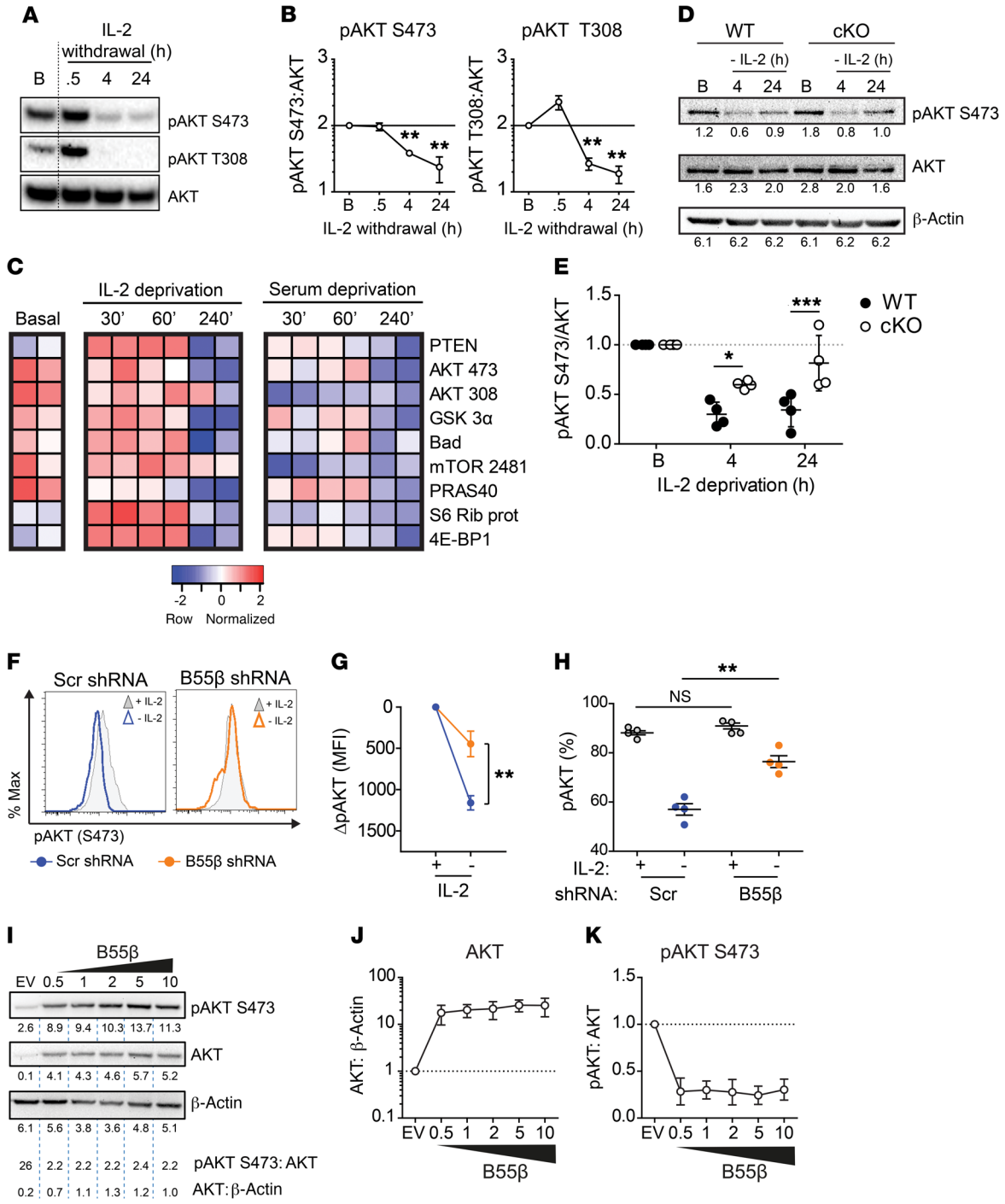

Figure 3. Cytokine withdrawal–induced AKT dephosphorylation depends on B55β. (**A**) Activated and expanded human T cells were resuspended in fresh RPMI (10% FBS) devoid of IL-2. AKT phosphorylation was assessed before (B) and after (0.5, 4, and 24 hours) cytokine withdrawal by Western blot. A representative blot is shown (n = 5). (**B**) Cumulative data of 5 experiments. Mean ± SEM of pAKT:AKT density is shown. $^{**}P \leq 0.01$ (paired 2-tailed t test). (**C**) Human T cells activated and expanded were lysed at the indicated time points. Phosphorylation of the enlisted proteins was analyzed by immunoblot (n = 2). (**D**) T cells from WT and cKO mice were activated and expanded. Cells were lysed at the indicated time points after IL-2 deprivation. AKT phosphorylation was quantified by Western blot. Densitometry is indicated under each blot. Two-way ANOVA with Bonferroni's multiple comparisons test; $^{*}P$ = 0.025, $^{***}P$ = 0.0006 (n = 4). (**F**) Human T cells were infected with B55β-specific or control shRNA-encoding lentiviruses. Cells were deprived of IL-2, and pAKT S473 was quantified by flow cytometry. Representative histograms: gray shades indicate pAKT prior and empty histograms pAKT after 8 hours of cytokine withdrawal. (**G**) Mean ± SEM of pAKT (S473) in cells infected with control (blue circles) or B55β-specific (orange circles) lentiviruses. Mean fluorescence intensity (MFI) was normalized to basal time point. Paired 2-tailed t test; $^{**}P \leq 0.01$. (**H**) The percentage of pAKT^{+} cells from **F** was quantified before (empty circles) and after IL-2 withdrawal (full circles). Each dot represents one sample. Two-tailed t test, $^{**}P$ = 0.001. (**I**) 293 T cells were transfected with a B55β-encoding plasmid (0.5–10 μg). Twenty-four hours later, cells were lysed and the indicated proteins were quantified by Western blotting. Densitometry is indicated. Cumulative data of 4 independent experiments showing AKT:β-actin (**J**) and pAKT:AKT (**K**) are shown.

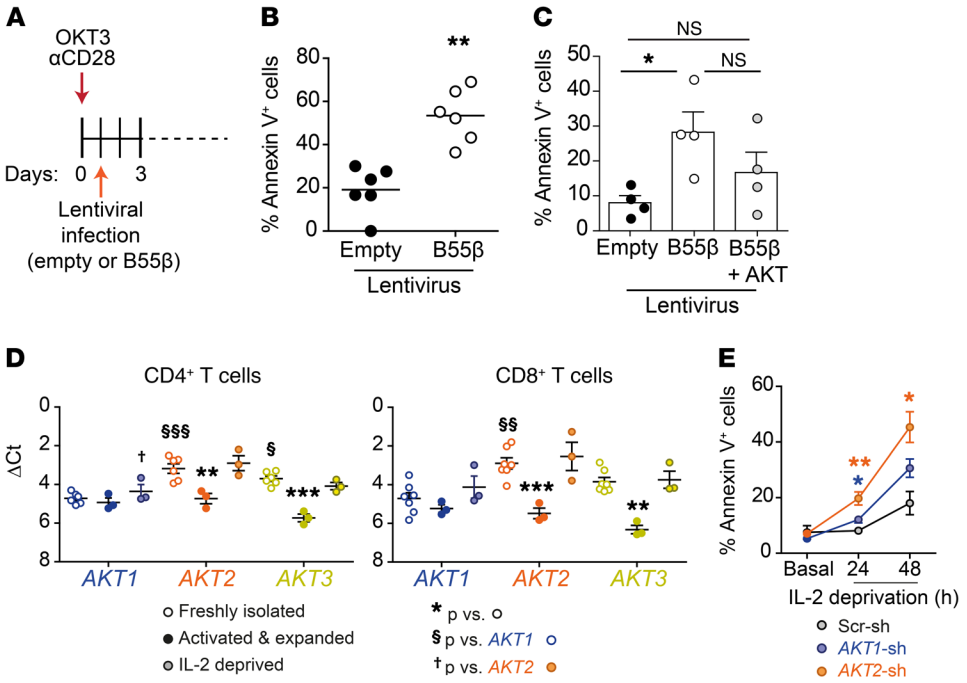

Figure 4. Apoptosis induced by B55β is blocked by AKT overexpression. (**A**) Schematic representation of in vitro stimulation and lentiviral infection of human T cells. (**B**) Apoptosis was quantified in human T cells infected with control- or B55β-encoding lentiviruses. Each dot represents a different sample (n = 6); line indicates mean. Paired 2-tailed t test was used; $^{**}P \leq 0.01$. (**C**) Human T cells were infected with control, B55β-encoding, or B55β-encoding plus AKT-encoding lentiviruses, and apoptosis was quantified by flow cytometry. Shown is the cumulative data (mean and SEM) of 4 independent experiments. One-way ANOVA with Dunn's multiple comparison test was used, $^{*}P < 0.05$. (**D**) *AKT1*, *AKT2*, and *AKT3* mRNA levels were quantified in human CD4$^+$ and CD8$^+$ T cells at the following time points: immediately after isolation (empty circles); after 7 days of activation (anti-CD3 + anti-CD28) and expansion in IL-2 (filled circles); 24 hours after IL-2 withdrawal (half-tone filled circles). Results are presented as ΔCt (vs. *ACTB*). $^{**}P < 0.01$ and $^{***}P < 0.001$ versus the same gene in freshly isolated cells; §$P < 0.05$ and §§§$P < 0.001$ versus *AKT1* in freshly isolated cells; †$P < 0.05$ versus *AKT2* in IL-2–deprived cells. One-way ANOVA with Bonferroni's multiple comparison test was used. (**E**) IL-2 deprivation was induced in cells infected with control, *AKT1*, and *AKT2* shRNA–encoding lentiviruses. Annexin V$^+$ cells were quantified at the indicated time points. $^{*}P < 0.05$ and $^{**}P < 0.01$ versus control (2-tailed paired Student's t test).

concentration of a T cell growth factor, we hypothesized that B55β triggers apoptosis through the modulation of the antiapoptotic function of AKT (25–27).

We activated and expanded T cells in vitro and then analyzed AKT phosphorylation in 2 residues that determine its activity (S473 and T308) (28, 29). Both residues of AKT were phosphorylated in activated T cells, but lost their phosphorylation 4 hours after IL-2 withdrawal (Figure 3, A and B). Serum deprivation causes AKT dephosphorylation and apoptosis in different cell lineages. To determine whether in vitro IL-2 withdrawal behaves in an analogous manner to serum deprivation, we analyzed the kinetics of dephosphorylation of AKT and other members of the AKT/mTOR pathway in activated T cells subjected to serum starvation or to IL-2 deprivation. As observed in other cell lineages, serum starvation induced rapid and profound dephosphorylation of the pathway (30, 31). Deprivation of IL-2 induced a similar response, but changes were only observed after a 4-hour time lag (Figure 3C) that corresponds to the upregulation of B55β induced by IL-2 withdrawal (15).

The kinetics of AKT dephosphorylation and B55β induction during cytokine withdrawal suggested that B55β might mediate AKT inactivation. To test this hypothesis, we compared AKT dephosphorylation in response to IL-2 withdrawal in T cells from WT and cKO mice. As shown in Figure 3, D and E, AKT dephosphorylation at 4 and 24 hours was significantly diminished in B55β-deficient T cells (4 hours: WT 0.3 ± 0.06 vs. cKO 0.6 ± 0.02, P = 0.02; 24 hours: WT 0.3 ± 0.08 vs. cKO 0.8 ± 0.14, P = 0.006). Next, we analyzed AKT phosphorylation in human T cells after B55β knockdown. As expected, IL-2 deprivation caused AKT dephosphorylation in cells infected with a control lentivirus. This effect was significantly prevented by B55β silencing (Figure 3F). When analyzed as MFI (Figure 3G) or as percentage of pAKT$^+$ cells (Figure 3H), B55β knockdown ameliorated AKT dephosphorylation in a statistically significant manner. Overexpression of B55β in 293T cells caused a significant drop in pAKT along with a reciprocal increase in the abundance of total AKT (Figure 3, I–K) that could represent a compensatory mechanism to decreased AKT activity. Interestingly, T cells deprived of IL-2 exhibit an increase in the levels of AKT at the mRNA level (Figure 4D), not reflected by changes at the protein level (Figure 3, A and D). This suggests that, as described for other genes, AKT is actively regulated at the translational level in activated T cells (32).

AKT inhibits apoptosis triggered by B55β. To determine whether the modulation of AKT phosphorylation is required for cell death to occur in response to B55β, we analyzed apoptosis in response to B55β forced expression. To this end, human T cells were activated and infected with control or B55β-encoding lentiviruses, and apoptosis was quantified by flow cytometry (Figure 4A). Annexin V binding was detected in a large fraction of the cells after infection with the B55β-encoding lentivirus (control 19.1 ± 4.4 vs. B55β 53.4 ± 5.1, P = 0.007) (Figure 4B). To test the role of AKT in B55β-

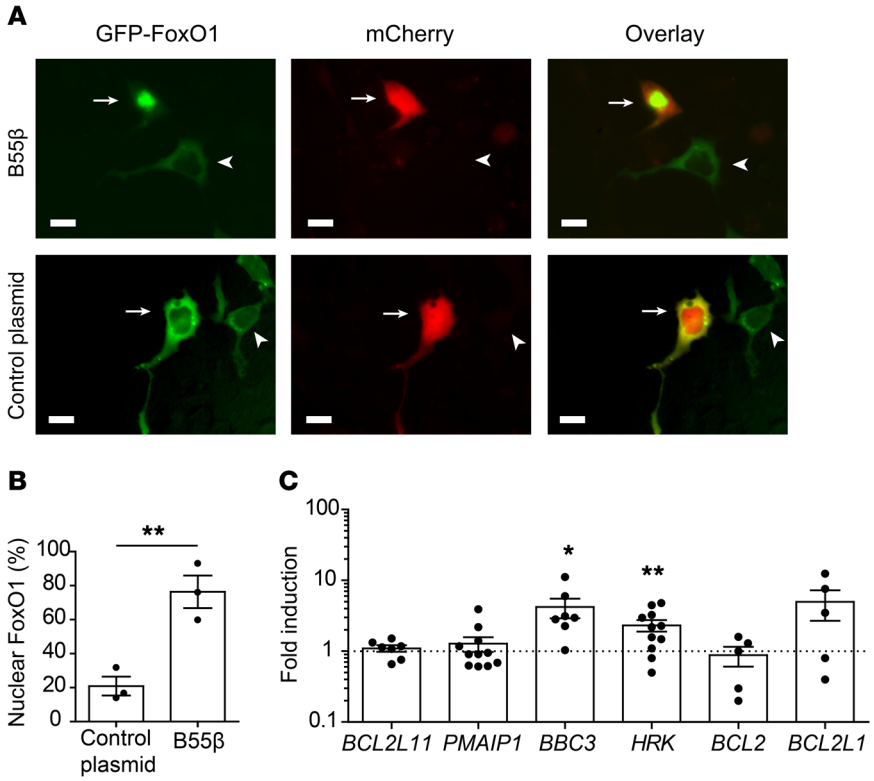

Figure 5. B55β activates FoxO1 and promotes *HRK* transcription. (**A**) MCF-7 cells were transfected with a plasmid encoding a GFP-FoxO1 fusion protein and either pLVX-*PPP2R2B*-IRES-mCherry or pLVX-mCherry, and FoxO1 localization was evaluated by fluorescence microscopy. Representative images are shown. Arrows indicate cells transfected with both plasmids; arrowheads indicate cells transfected only with GFP-FoxO1. Scale bars: 5 μm. (**B**) Cumulative data (mean ± SEM) of 3 independent experiments are shown (each dot represents 1 experiment). In each experiment, 100 cotransfected cells were evaluated. For comparison of the means, unpaired 2-tailed *t* test was used; $^{**}P \leq 0.01$. (**C**) Human T cells were infected with control- or B55β-encoding lentiviruses following the procedure depicted in Figure 4. Sixteen hours later, expression of the indicated genes was quantified by real-time PCR and normalized to *ACTB*. Cumulative data of 8 independent experiments expressed as mean ± SEM fold induction against empty virus (indicated by the broken line). Each dot represents 1 sample. For comparison of the means, unpaired 2-tailed *t* test was used; $^{*}P \leq 0.05$, $^{**}P \leq 0.01$.

induced apoptosis, we infected T cells with B55β/mCherry and either control GFP or AKT/GFP-encoding lentiviruses, and analyzed apoptosis in mCherry/GFP-coexpressing cells. As shown in Figure 4C, forced expression of AKT tended to decrease B55β-induced cell death (B55β 28.25 ± 5.8 vs. B55β + AKT 16.7 ± 5.8, *P* = NS). In humans and mice, AKT has 3 isoforms (AKT1, AKT2, and AKT3) encoded by 3 highly homologous genes (33). We analyzed the expression of the 3 genes in $CD4^+$ and $CD8^+$ T cells and found that *AKT2* and *AKT3* are the predominant isoforms in resting cells (Figure 4D). However, during T cell activation and expansion, *AKT2* and *AKT3* are downregulated and the 3 isoforms are transcribed at roughly the same level. IL-2 deprivation stimulates the transcription of *AKT2* and *AKT3,* and 24 hours after IL-2 deprivation, *AKT2* is the most highly expressed isoform in $CD4^+$ and $CD8^+$ T cells (Figure 4D). *AKT2* silencing significantly increased the rate of apoptosis induced by cytokine withdrawal (Figure 4E), and *AKT2* (but not *AKT1*) levels significantly correlated with apoptosis rate in cells deprived of IL-2 ($R = 0.64$, $P = 0.03$; Supplemental Figure 8). These results suggest that AKT2 may represent the AKT isoform that promotes T cell survival during growth factor withdrawal. Taken together, these data indicate that B55β induced during IL-2 withdrawal promotes AKT dephosphorylation, which hampers the prosurvival capacity of AKT and triggers apoptosis.

B55β promotes FoxO transcriptional activity. Forkhead box O (FoxO) transcription factors regulate several cellular processes including apoptosis (34). Phosphorylation by AKT (35, 36) inhibits the transcriptional activity of FoxO factors by promoting their association with 14-3-3 proteins and consequently their sequestration in the cytoplasm (37).

To determine whether AKT inactivation in response to B55β expression modifies the regulation of FoxO factors, we cotransfected MCF-7 cells with a plasmid encoding a GFP-FoxO1 fusion protein (38) and either an mCherry control or an mCherry/B55β-encoding plasmid (Figure 5A). FoxO1 localized mainly in the cytoplasm and was found in the nucleus of only approximately 20% of the cells transfected with a control plasmid. In contrast, cotransfection of B55β caused FoxO1 nuclear translocation in a majority of the cells (control 20.9 ± 5.6 vs. B55β 76.4 ± 9.6, *P* = 0.007, Figure 5B).

Next, we infected human T cells with control or B55β-encoding lentiviruses and measured the expression of FoxO-regulated genes by quantitative PCR (qPCR). To this end, we chose *BCL2L11* (Bim), *PMAIP1* (Noxa), *BBC3* (PUMA), *HRK*, *BCL2*, and *BCL2L1* (Bcl-$_{XL}$), because they are regulated by FoxO factors and/or involved in apoptosis (39, 40). As shown in Figure 5C, forced expression of B55β in T cells specifically induced the transcription of *BBC3* (p53 upregulated modulator of apoptosis [PUMA]) and *HRK* (Harakiri) in a significant manner. Transcription of other apoptosis-related genes (i.e., *BIM*, *PMAIP1*, *BCL2*, and *BCL2L1*) was not consistently modified by the ectopic expression of B55β in T cells.

B55β is required for the upregulation of Hrk during cytokine withdrawal. Hrk (Harikiri or Dp5) is a proapoptotic Bcl-2-homolog 3–only (BH3-only) protein of the Bcl-2 family (41). *Hrk* was first identified by differential display screening in neurons undergoing apoptosis induced by neuronal growth factor deprivation (42). More recent work determined that HRK is necessary for apoptosis of diffuse large B cell lymphoma cells in response to inhibition of the PI3K/AKT/FoxO1 survival pathway (43, 44). Because expression of Hrk was induced by forced expression of B55β (Figure 5C), we hypothesized that it may represent the main proapoptotic molecule responsible for the cell death–inducing effects of B55β. To test whether B55β is necessary for Hrk induction during CWID, we subjected activated T cells from WT and cKO mice to cytokine withdrawal. As expected, IL-2 deprivation caused an upregula-

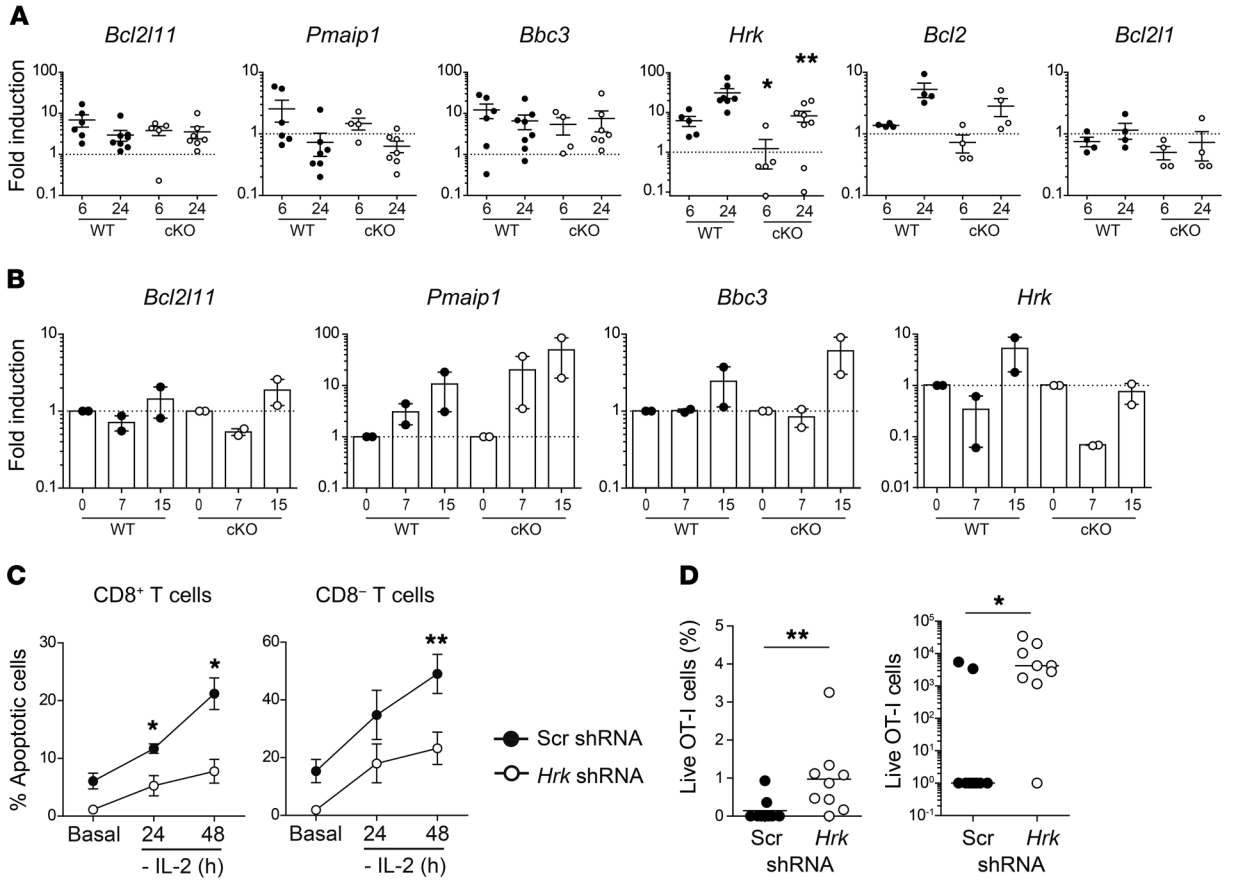

Figure 6. B55β-induced *Hrk* is essential for CWID. (**A**) T cells from *Ppp2r2b*$^{+/+}$*Cd4*.Cre^{+} (WT) or *Ppp2r2b*$^{fl/fl}$*Cd4*.Cre^{+} (cKO) mice were activated and expanded in vitro. Expression of the indicated genes was assessed by qPCR before (basal) and after 6 and 24 hours of cytokine withdrawal. Cumulative data from 4 experiments (n = 3–4 mice/group/experiment) are shown. Mean and SEM are indicated. *$P \le 0.05$, **$P \le 0.01$ (unpaired 2-tailed Mann-Whitney test). (**B**) WT or cKO OT-I cells were adoptively transferred into CD45.1^{+} mice. Next day, LM-OVA was injected into recipient mice. RNA was extracted from sorted cells (CD45.2^{+} CD8^{+} Vα2^{+} Vβ5^{+}) at days 7 and 15 and qPCR was performed. Results are presented as mean and SEM. Cumulative data from 2 independent experiments (n = 3–5 mice/group/experiment) are shown. In **A** and **B**, the dotted line indicates the expression level of the basal sample. (**C**) T cells from WT mice were activated and infected with control (Scr) or Hrk-shRNA encoding lentiviruses. Cells were expanded and apoptosis was induced by cytokine withdrawal. GFP^{+} (effectively infected) apoptotic cells were quantified. Cumulative data from 2 experiments (n = 4 mice/group/experiment). *$P \le 0.05$, **$P \le 0.01$ (unpaired 2-tailed t test). (**D**) CTLs from OT-I WT or cKO mice were infected with a control (Scr-Cerulean) or an Hrk-specific shRNA encoding lentivirus (GFP). Six days later, 1.6 × 10^{4} Cerulean^{+} and GFP^{+} OT-I T cells were injected at a 1:1 ratio into RIP-mOVA mice. Fourteen days later, relative and absolute numbers of transferred cells (Cerulean or GFP^{+}) were quantified (n = 9). *$P \le 0.05$, **$P \le 0.01$ (unpaired 2-tailed Mann-Whitney test).

tion of Bim (*Bcl2l11*), Puma (*Pmaip1*), Noxa (*Bbc3*), *Bcl2*, and *Hrk*. Absence of B55β was associated with a modest, nonsignificant reduction in the expression of Bim, Puma, Noxa, Bcl2, and Bcl-$_{XL}$ at 6 and 24 hours after IL-2 deprivation. In contrast, B55β deficiency abolished the upregulation of *Hrk* at 6 (WT 6.2 ± 1.8 vs. cKO 1.2 ± 0.9, P = 0.035) and 24 hours (WT 31.1 ± 8.6 vs. cKO 8.2 ± 2.5, P = 0.018) (Figure 6A). To assess the relevance of these findings in the in vivo system, we adoptively transferred WT and cKO OT-I cells into CD45.1^{+} mice and infected them with LM-OVA. At days 7 and 15, we sorted the transferred CD45.2^{+} OT-I cells and analyzed the expression of Bim, Puma, Noxa, and Hrk. As shown in Figure 6B, upregulation of the 4 proapoptotic genes was detected at day 15 p.i. in WT cells. Although the kinetics of expression of Bim, Puma, and Noxa were maintained in the absence of B55β, induction of Hrk was completely abolished in cKO cells.

The mitochondrial pathway of apoptosis is a complex process that involves several proteins. To weigh the individual importance of Hrk, we evaluated the effect of its silencing in cells subjected to CWID. As shown in Figure 6C, Hrk knockdown significantly decreased apoptosis induced by IL-2 deprivation in CD8^{+} and in CD8^{-} T cells. To test the in vivo significance of these findings, OT-I T cells infected with either a control lentivirus encoding a blue fluorescent protein (Cerulean) or a B55β-specific shRNA (plus GFP) were mixed in a 1:1 ratio and adoptively transferred into RIP-mOVA mice. After 14 days, the mice were sacrificed and the survival of the transferred cells was compared. Cells infected with the control virus were undetectable in most mice. In contrast, *Hrk* knockdown was associated with a significant increase in the number of live transferred cells (control shRNA 990 ± 677 vs. *Hrk* shRNA 8813 ± 3839, P = 0.039) (Figure 6D).

Taken together, these results indicate that Hrk plays an essential and nonredundant role in the induction of CD8^{+} T cell apoptosis during cytokine withdrawal. Thus, declining IL-2 abundance promotes the transcription of B55β, AKT regulation, and FoxO transcriptional activation, which culminates with Hrk production and apoptosis.

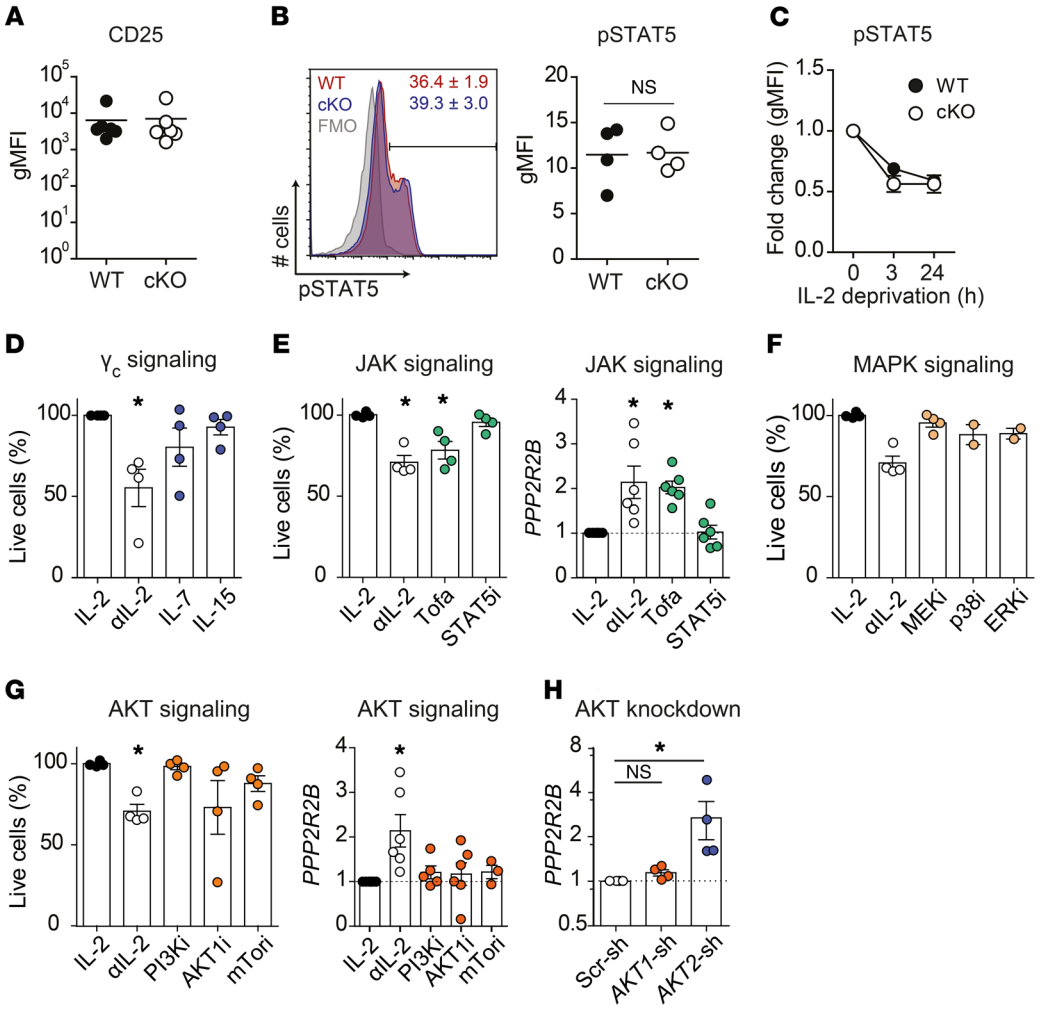

Figure 7. AKT2 inhibits B55β expression. (**A**–**C**) *Ppp2r2b*$^{+/+}$ (WT) or *Ppp2r2b*$^{fl/fl}$ (cKO) T cells were activated and expanded in the presence of IL-2 for 10 days. (**A**) CD25 (IL-2Rα) expression on activated WT and cKO T cells. (**B**) STAT5 (Y694) phosphorylation in the presence of IL-2 (10 U/mL). A representative histogram and cumulative data from 2 independent experiments are shown. $P = 0.46$, unpaired *t* test. (**C**) STAT5 phosphorylation in WT and cKO mice upon IL-2 withdrawal. Data are expressed as mean ± SEM. Two independent experiments ($n = 2$ per group, per experiment). (**D**–**G**) Activated and expanded T cells were deprived of IL-2 (αIL-2) in the absence or presence of other cytokines, or were maintained in IL-2 while exposed to specific inhibitors. Live cells were quantified after 48 hours and compared with cells not deprived of IL-2 (IL-2). *PPP2R2B* mRNA levels were quantified 24 hours after IL-2 deprivation or after addition of inhibitors. (**D**) The effect of IL-7 (15 ng/mL) or IL-15 (20 ng/mL) was analyzed in cells deprived of IL-2. (**E**) Cells were incubated with tofacitinib (Tofa; 100 nM) or STAT5i (25 μM). (**F**) Cells were exposed to PD98039 (MEKi, 10 μM), SB202190 (p38i, 1 μM), or FR180204 (ERKi, 20 μM). (**G**) Cells were incubated with LY294002 (PI3Ki, 2 μM), MK-2206 (AKTi, 2 μM), or rapamycin (mTORi, 500 nM). Three independent experiments ($n = 1$–2 per experiment). Kruskal-Wallis test with Dunn's multiple comparison analysis was used. *$P < 0.05$. (**H**) T cells were activated and infected with lentiviruses encoding shRNAs (scrambled, *AKT1*-, or *AKT2*-specific). *PPP2R2B* expression was quantified by qPCR. Four independent experiments ($n = 1$ per experiment). Friedman test with Dunn's multiple comparison analysis was used. *$P < 0.05$.

Signaling through AKT2 inhibits B55β expression. Deficient expression of *Ppp2r2b* could alter IL-2 signaling, conferring resistance to CWID. To examine this possibility, first we compared the expression levels of CD25, the alpha subunit of the IL-2 receptor. As shown in Figure 7A, WT and cKO T cells displayed comparable levels of CD25. Likewise, the response of WT and cKO cells to IL-2, measured as STAT5 phosphorylation, was also similar in the absence of B55β (Figure 7B). Finally, the kinetics of STAT5 phosphorylation during IL-2 deprivation were also normal in cKO T cells (Figure 7C). These data indicate that proximal signaling through the IL-2 receptor is not affected by B55β deficiency.

IL-2 signaling activates at least 3 pathways: JAK1/3/STAT5, PI3K/AKT/mTORC1, and MAP kinases (45). To determine whether one of these pathways is primarily involved in the regulation of T cell survival during low cytokine conditions, we dissected their contribution to B55β induction and cell death. IL-7 and IL-15, 2 cytokines that signal through the common γ chain receptor (γ_c) and JAK3, rescued T cells from apoptosis induced by IL-2 withdrawal (Figure 7D), confirming that signaling through γ_c is necessary for activated T cell survival (46). Accordingly, exposure to Tofacitinib, a JAK1/3 inhibitor, induced apoptosis in the presence of IL-2 and promoted the transcription of *PPP2R2B* at comparable levels than IL-2 withdrawal (Figure 7E). Specific inhibition of STAT5 did not cause cell death, nor *PPP2R2B* transcription (Figure 7E), and a comparable lack of effect was observed when PI3K, mTORC1, MEK, p38, and ERK were inhibited using a pharma-

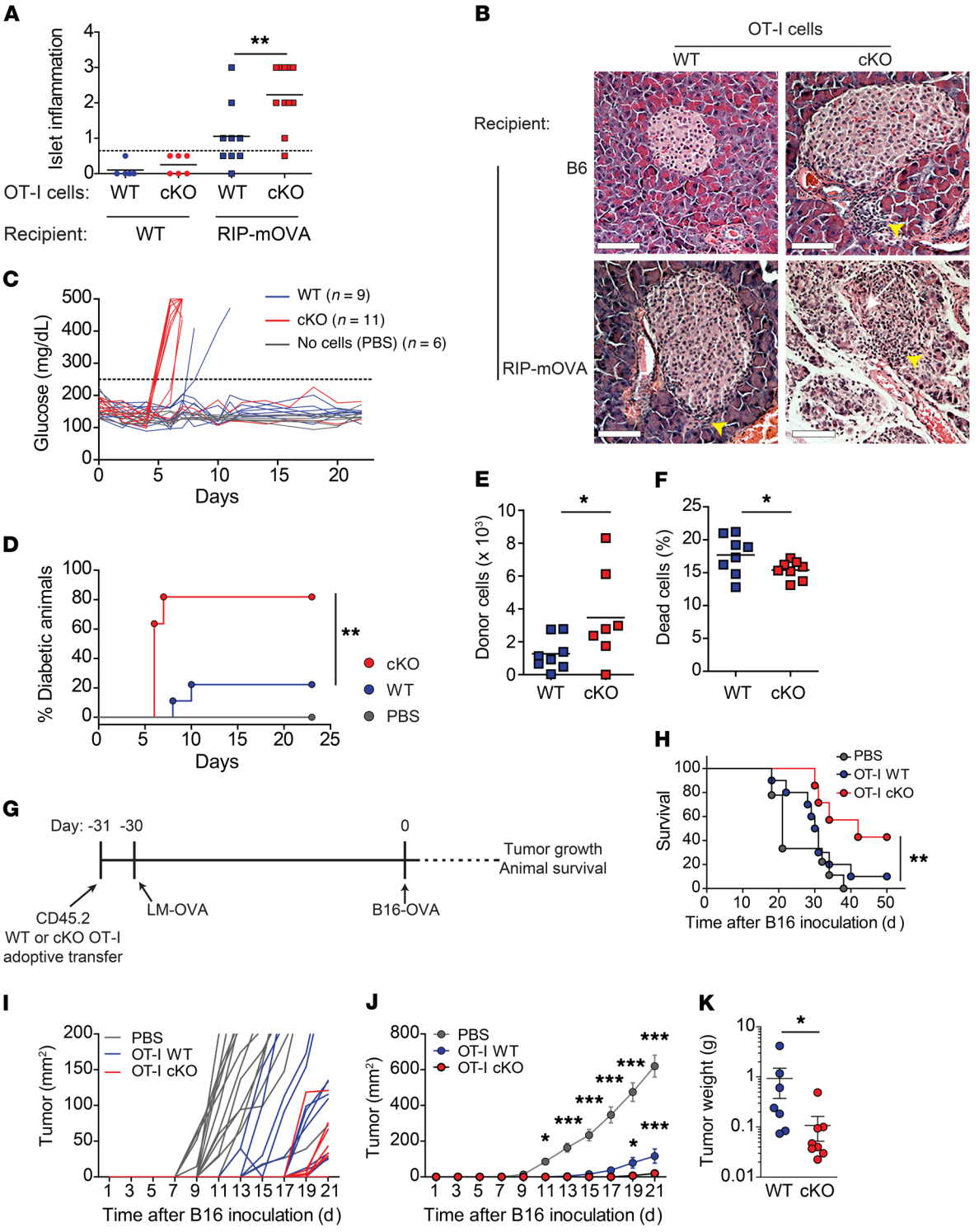

Figure 8. B55β controls the pathogenic capacity of CD8⁺ T cells. (**A**–**F**) OT-I cells differentiated into CTLs. After 4 days, they were i.v. injected into RIP-mOVA or WT mice. Blood glucose was quantified every day. (**A**) Pancreatic inflammation was scored: 0, no inflammation; 1, small perivascular infiltrates; 2, inflammatory infiltrates surrounding the islets; 3, inflammatory infiltration and/or destruction of the islets. Cumulative data of 2 independent experiments (n = 4–6 mice per group) are shown. Unpaired t test, $^{**}P \le 0.01$. (**B**) Representative images of H&E-stained pancreata from **A** are shown. Arrowheads indicate inflammatory infiltrates. Scale bars: 100 μm. (**C**) Glucose levels in RIP-mOVA mice that received WT or cKO OT-I CTL, or PBS. Cumulative data from 2 independent experiments are shown. (**D**) Incidence of diabetes in RIP-mOVA mice (n = 4–6 mice per group). Log-rank (Mantel-Cox) test, $^{**}P \le 0.01$. (**E**) Transferred cells ($CD45^+CD8^+V\alpha2^+V\beta5^+CD44^+$) in draining lymph nodes and pancreata of recipient RIP-mOVA mice 5 days after CTL transfer. Cumulative data of 2 experiments (n = 3–5 mice per group). Unpaired t test, $^{*}P \le 0.05$. (**F**) Dead donor cells ($GhostDye^+$) in the spleens of recipient mice after CTL transfer. Cumulative data from 2 experiments (n = 3–5 mice per group). Unpaired t test, $^{*}P \le 0.05$. (**G**–**K**) A quantity of 10^6 OT-I CD45.2 *Ppp2r2b*$^{+/+}$ or *Ppp2r2b*$^{fl/fl}$ were adoptively transferred into CD45.1 mice. The next day, 10^4 CFU of LM-OVA were i.v. injected into the recipient mice. After 30 days, 2×10^5 B16-OVA melanoma cell line cells were implanted in the left flanks of the animals (**G**). Survival (**H**) and tumor growth (**I**–**J**) were monitored. (**K**) Tumor weight on day 21. Cumulative data from 2 experiments (n = 3–5 mice per group). One-way (**H**) and 2-way (**J**) ANOVA and unpaired t test (**K**) were used. Mean ± SEM is depicted. $^{*}P \le 0.05$; $^{**}P \le 0.01$; $^{***}P \le 0.001$.

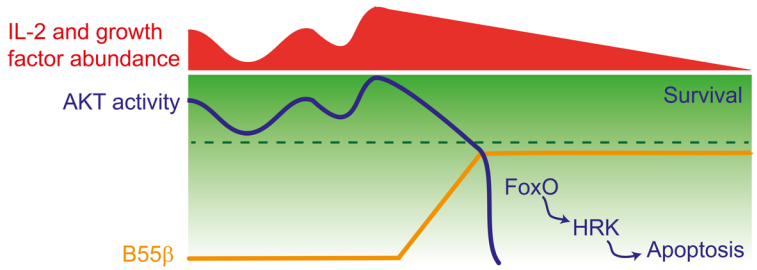

Figure 9. Decreased AKT activity induces B55β transcription, which halts further AKT activation. AKT activity fluctuates in response to nutrient and growth factor abundance. When AKT activity decreases under a certain threshold (indicated by the broken line), for example, during IL-2 withdrawal or AKT silencing, expression of B55β is induced. By promoting AKT dephosphorylation, B55β actively inhibits further AKT activity and commits the cell to apoptosis through the activation of FoxO and the induction of HRK.

cologic approach (Figure 7, F and G). Addition of the AKT inhibitor, MK-2206, caused inconsistent results. In some experiments, MK-2206 induced cell death in the presence of IL-2, whereas in other experiments, it had no effect (Figure 7G). MK-2206 exerts a differential effect on each AKT isoform (47) and the variations observed could be caused by differential inhibition of the different AKT isoforms. To explore this possibility, we silenced *AKT1* or *AKT2* and quantified B55β transcription. As shown in Figure 7H, *AKT1* knockdown had no effects on *PPP2R2B* mRNA abundance. In contrast, *AKT2* knockdown was associated with a significant increase in B55β expression. These data, which are consistent with the increase in apoptosis observed in T cells following *AKT2* silencing (Figure 4E), suggest that AKT2 signaling promotes activated T cell survival during cytokine withdrawal by inhibiting B55β expression.

B55β curbs the pathogenic capacity of CD8⁺ T cells. Defects in the contraction of activated T cells can contribute to immunopathology and autoimmune disease. To determine the relevance of the B55β-regulated apoptotic pathway, we differentiated OT-I cytotoxic T lymphocytes (CTLs) and transferred them into mice that express OVA in the pancreatic β cells (RIP-mOVA). Absence of B55β was associated with severe pancreatic islet inflammation and early development of diabetes in 80% of the animals. In contrast, B55β-sufficient cells caused mild inflammation and diabetes in only 20% of the mice (Figure 8, A–D). To determine whether the heightened pathogenicity of B55β cKO T cells could be attributed to enhanced effector function, we compared proliferation, granzyme B expression, degranulation, and cytotoxic capacity between WT and cKO CD8⁺ T cells. As shown in Supplemental Figure 9, we found no differences in these parameters, suggesting that the increase in tissue damage derived from their enhanced survival. In support of this hypothesis, we found that the survival of cKO OT-I CTLs transferred to RIP-mOVA mice was significantly higher than the survival of WT OT-I CTLs (Figure 8, E and F).

To assess the relevance of the B55β-associated increase in CD8⁺ T cell survival, we transferred CD45.2 OT-I cells (WT or cKO) into CD45.1 mice and infected them with LM-OVA. Thirty days later, mice were inoculated with a melanoma cell line that expresses OVA (B16.OVA) and survival and tumor growth were monitored (Figure 8G). As shown in Figure 8, H–K, cKO OT-I cells dealt with the OVA-expressing melanoma in a significantly more efficient manner. Mice that received cKO cells were more likely to survive (43% vs. 10% survival at day 50, $P = 0.008$, Figure 8H) and tumor growth was importantly retarded (Figure 8, I–K). Because lack of B55β does not affect the effector function of CD8⁺ T cells, the heightened response to OVA-bearing tumor cells reflects a more robust memory response associated with increased CD8⁺ memory T cell lifespan.

Discussion

The factors that determine when an activated T cell will terminate its functional life and activate the mechanisms that will lead to its apoptotic death remain poorly understood. Elements external to the cell, such as abundance of cytokines and growth factors, persistence of antigenic stimulation, and the action of regulatory T cells, have been identified as triggers that precipitate apoptosis in activated T cells through the mitochondrial pathway (17, 20). The importance of each of these factors has been demonstrated by experimental manipulation. For example, genetic deletion of Bim decreased the rate of clonal contraction during acute infections (48). How these external factors are integrated by the cell and translated into a death signal has remained unknown (49). Our results introduce B55β as a key player in this process.

Expression and function of B55β is intimately associated with the pathways that sense the external milieu, in particular abundance of nutrients and growth factors, and implement customized metabolic adaptations. Transcription of B55β is set in motion by reduced AKT2 activity and its main effect is to terminate AKT activity. Thus, presence of B55β may signal commitment to apoptosis and a transition to a state where prosurvival factors can no longer rescue the cell. AKT activity may fluctuate in response to variations in the frequency and intensity of the stimuli that it senses. It is possible that when such fluctuations reach the threshold where B55β is elicited, its AKT-regulating function may inhibit further teetering and by shutting off the pathway actively terminate the prosurvival capacities of AKT, block further AKT activation, and initiate apoptosis (Figure 9). How different AKT-activating stimuli differentially affect AKT function in T cells is unknown and warrants further investigation. Our combined in vivo and in vitro approaches were not designed to dissect the contribution of the different cues that modulate AKT activity. By depriving activated T cells from IL-2, we were able to observe B55β expression followed by the events that culminate in cell death. However, the relative importance of decreased cytokine availability in the complex in vivo setting remains unclear. The fact that B55β deficiency prolongs the lifespan of antigen-specific CD8⁺ T cells and inhibits the expression of Hrk indicates that our in vitro system recapitulates to some extent the events that trigger cell death in vivo, but as with any reductionist approach, it may lack depth and complexity when compared with the phenomenon occurring in a natural setting.

AKT represents a family of 3 highly homologous kinases (AKT1 or PKBα, AKT2 or PKBβ, and AKT3 or PKBγ) (33, 50) that play an essential role as prosurvival kinases in different situations and in

different cell lineages, including healthy (51) and transformed B cells (43). Transgenic expression of myristoylated (constitutively active) AKT1 is associated with increased survival of thymocytes and peripheral T cells during cytokine withdrawal (52, 53). On the other hand, the 3 isoforms have been shown to promote thymocyte survival in mice with 1 or more AKT genes deleted, suggesting that the 3 AKT kinases may exert partially redundant prosurvival activities in immature and mature T cells (54, 55). Our data offer a glimpse at the complexity of this system, as they show that the 3 isoforms are dynamically regulated during quiescence, cell cycle, and cytokine withdrawal. They further support AKT2 as a major contributor to cell survival during cytokine deprivation, but further studies are required to determine the exact contribution of each AKT isoform to this process and to determine whether B55β affects the activity of all or individual AKT isoforms.

The regulation of the mitochondrial pathway of apoptosis is a complex process where several cellular stresses (e.g., cytokine deprivation, DNA damage) converge to trigger death (56). This pathway is mainly controlled by interactions between Bcl-2 and a family of related proteins. Cellular stresses promote the expression of proapoptotic BH3-only proteins (i.e., Bim, Bad, Puma, Noxa, Hrk) that neutralize Bcl-2 and other antiapoptotic proteins (e.g., Bcl-$_{XL}$) allowing the activation and oligomerization of Bax and Bak, which form pores on the mitochondrial outer membrane (57). The functions of BH3-only proteins are redundant and loss of individual molecules tend to have mild consequences (57). Different cellular stresses induce different BH3-only proteins. For example, DNA damage is associated with expression and activation of Puma and Noxa (58, 59). Using overexpression and knockout systems, we have shown that Hrk is induced in T cells by cytokine deprivation in a B55β-dependent manner. Hrk was first shown to play a proapoptotic role in neurons deprived of NGF (42). Later work suggested that Hrk was also induced by growth factor withdrawal in hematopoietic precursors (60), but this notion was later challenged by findings in an Hrk-deficient mouse (61). Our data demonstrate that in activated T cells, B55β expression robustly induces Hrk transcription. Further, we demonstrate that B55β is necessary for Hrk transcription in response to cytokine withdrawal and that this BH3-only protein plays a nonredundant role during T cell CWID. These results are in concordance with Chen et al., who observed Hrk expression in B cell blasts treated with inhibitors of the AKT pathway (43).

As reported in mice deficient in other molecules involved in the regulation of the mitochondrial apoptosis pathway (58, 59, 62, 63), absence of B55β did not cause a strong spontaneous phenotype. Intriguingly, it was primarily associated with the accumulation of activated CD8$^+$ T cells that express CD62L and IFN-γ. The apparent differences in the effects that B55β deficiency exerts on CD4$^+$ and CD8$^+$ T cells may be caused by intrinsic differences in apoptosis sensitivity, by different cell expansion and contraction kinetics, or by the fact that CD4$^+$ and CD8$^+$ T cells are not equally susceptible to IL-2 deprivation caused by Tregs (22). T cell activation is associated with downregulation of B55β (15), but resting memory CD8$^+$ T cells express higher levels of B55β than their naive counterparts (16). Upregulation of B55β could render memory CD8$^+$ T cells particularly susceptible to apoptosis induced by growth factor withdrawal, while the abundance of other pro- and antiapoptotic molecules could modulate their sensitivity to apoptosis. For instance, differential amounts of Bcl-2 and Bcl-$_{XL}$ in EM and CM T cells (64), or differences in Bim expression and in the regulation of protective autophagy (65) may render CM T cells more resistant to B55β-mediated death in the setting of CWID. Increased abundance of IL-7 and IL-15 receptors on memory T cells and precursors may promote the survival of these cells by inhibiting B55β expression through γ_c signaling. These aspects emphasize the fact that B55β acts in a cellular context where other unknown factors may modulate its expression, function, and downstream effects. For example, a recent work from our group described how chronic inflammation confers T cells resistant to apoptosis in patients with systemic autoimmune diseases by inhibiting the transcription of B55β through an epigenetic mechanism (16).

Adoptive transfer of activated and expanded CD8$^+$ T cells (CTLs) into mice that express their cognate antigen in the pancreatic β cells was pathogenic only in the absence of B55β. This effect did not depend on the acquisition of better effector capacities but on the prolonged lifespan conferred by B55β deficiency. This model is relevant because it demonstrates that abnormal survival of activated T cells can lead to a breach in tolerance in otherwise healthy organisms. It is also relevant in the setting of cancer immunotherapy, where the ability of transferred effector cells depends on their capacity to survive in an environment where cytokines are relatively scarce (66). B55β silencing or deletion might represent an effective means to overcome this problem, because other solutions, such as administration of exogenous IL-2, have demonstrated only limited success and important secondary effects, such as IL-2–induced toxicity and regulatory T cell expansion (66). The fact that B55β deficiency allowed antigen-specific CD8$^+$ T cells to confer enhanced protection against melanoma further supports the notion that inhibition of this pathway may allow longer-lived T cell immune responses, which may prove useful in certain situations.

In summary, our work demonstrates that the PP2A regulatory subunit B55β represents a molecular link that commits activated T cells to apoptosis in response to cytokine deprivation through a conserved pathway that involves AKT, FoxO, and HRK. The understanding of this molecular mechanism could have broad implications in our capacity to modulate the length of immune responses in the setting of autoimmunity, cancer, and vaccination.

Methods

Antibodies, reagents, cell lines, plasmids

Detailed information of plasmids, antibodies, and reagents is provided in Supplemental Tables 1–3. LeGo plasmids (67) were a gift from Boris Fehse (University of Hamburg, Hamburg, Germany). pWPI, psPAX2, and pMD2.G plasmids were a gift from Didier Trono (École Polytechnique Fédérale de Lausanne, Lausanne, Switzerland). GFP-FoxO1 plasmid was a gift from Domenico Accili (Columbia University, New York, New York, USA). MCF-7 and HEK293T/17 cell lines were purchased from ATCC. B16-F10/OVA cells were a gift from Laura Bonifaz (Instituto Mexicano del Seguro Social, Mexico City, Mexico). Cells were maintained at 37°C, 5% vol/vol CO_2, in a humidified incubator in DMEM supplemented with 10% FBS, 2 mM L-glutamine, and 200 U/mL penicillin-streptomycin.

Animal models

Mice used in this study were housed in specific pathogen–free conditions on a 12-hour light/12-hour dark cycle. Mice had ad libitum access to food and water throughout the study. No previous procedure had been performed in the animals. Mice were randomly assigned to the experimental groups. The *Ppp2r2b*$^{fl/fl}$ mouse strain used in this research project was generated by KOMP and obtained from the KOMP Repository (www.komp.org). CD8$^+$ T cells from OT-I *Ppp2r2b*$^{fl/fl}$.*Cd4*-Cre or *Ppp2r2b*$^{+/+}$.*Cd4*-Cre mice were isolated using CD8α$^+$ T Cell Isolation Kit II (Miltenyi Biotec) according to the manufacturer's instructions.

Infection with Listeria. Cells (1×10^6) were injected i.v. into the lateral tail vein of CD45.1 recipient mice. One day after, 10^4 CFU *Listeria monocytogenes* expressing recombinant OVA (LM-OVA; a gift from Michael J. Bevan, University of Washington) were injected i.v. (68). At the indicated times after infection, splenocytes were isolated and analyzed using flow cytometry. To determine cytokine production, 5×10^6 splenocytes were cultured at 37°C for 5 hours in complete RPMI 1640 medium with 1 μL/mL Brefeldin A (BD Biosciences) and stimulated with SIINFEKL (1 μg/mL). After culture, cells were harvested and stained using BD Biosciences Cytofix/Cytoperm Fixation/Permeabilization Kit. All FACS data were acquired using a BD Biosciences LSR Fortessa and analyzed using FlowJo software (Tree Star). To determine bacterial load in infected mice, animals were sacrificed and perfused with 10 mL cold PBS. Livers were removed and mashed in 1% saponin. Dilutions were plated on brain-heart infusion agar supplemented with 10 mg/mL chloramphenicol and grown for 2 days at 37°C (69).

Induction of diabetes. Spleen cells from *Ppp2r2b*$^{+/+}$ OT-I (WT) or *Ppp2r2b*$^{fl/fl}$ OT-I (cKO) mice were differentiated to CTLs after RBC lysis in the presence of 0.5 μg/mL SIINFEKL and 100 U/mL rhIL-2 for 4 days (culture medium and IL-2 were replenished every other day). On day 4, CD8$^+$ T cells were isolated by negative selection, and 2.5×10^5 CD8$^+$ CTLs were adoptively transferred into the lateral tail vein of RIP-mOVA mice. Blood glucose was measured every other day and mice were euthanized after 2 consecutive readings of blood glucose 250 mg/dL or greater. Pancreata were collected, fixed in 10% formaldehyde, and prepared for histological analyses.

Memory response. After WT or cKO OT-I cell adoptive transfer, CD45.1 mice were infected with LM-OVA as detailed above. Thirty days later, mice received a subcutaneous injection of OVA-expressing B16 melanoma cells (2×10^5). Animals were monitored every 2 days. Tumor size was calculated by using the following formula: tumor size (mm^2) = (length) × (width) × π. Mice with tumor 800 mm^2 or greater were sacrificed.

In vitro expansion of T cells and induction of CWID

Human cells. We adapted a protocol published by Snow et al. (21). T cells were isolated from peripheral blood mononuclear cells using magnetic beads and stimulated in RPMI 1640 medium containing 10% of FBS, 2 mM L-glutamine, and 200 U/mL penicillin-streptomycin. T cell activation was performed with plate-bound anti-CD3 (5 μg/mL) and anti-CD28 (2.5 μg/mL). After 72 hours, cells were transferred into new plates, RPMI was duplicated, and rhIL-2 (100 U/mL) was added. RPMI and rhIL-2 were duplicated every 48 hours. At day 10 of cell culture, T cells were washed in cold PBS and replated in complete RPMI without IL-2. At the indicated times, cells were stained for apoptosis quantification or lysed in TRIZol to obtain RNA.

Murine cells. Cells were isolated from axillary and inguinal lymph nodes from *Ppp2r2b*$^{fl/fl}$.*Cd4*-Cre or *Ppp2r2b*$^{+/+}$.*Cd4*-Cre mice and as previously indicated for human cells. T cell activation was performed with plate-bound anti-CD3 (2 μg/mL) and anti-CD28 (2 μg/mL). At day 10 of cell culture, T cells were washed in cold PBS and replated in complete RPMI without IL-2, in the presence of anti-mouse IL-2 (5 μg/mL). At the indicated times, cells were stained for apoptosis quantification or lysed in TRIZol to obtain RNA.

Flow cytometry

All in vitro experiments were performed in triplicate for each condition, and the presented data are representative of at least 2 independent experiments. To assess apoptosis, human or mouse T cells were washed in cold PBS and stained with fluorescently labeled antibodies (i.e., CD3, CD4, CD8) for 15 minutes. Then, cells were washed and resuspended in Annexin V binding buffer (BioLegend) containing Annexin V and 5 nM Sytox Orange (Thermo Fisher Scientific). Ten minutes later, they were analyzed by flow cytometry. In some experiments, caspase activation was evaluated using the FAM-FLICA assay kit (Immunochemistry Technologies) following the manufacturer's instructions. Briefly, cells were stained with Ghost Dye Red 780 (Tonbo Biosciences) in ice-cold PBS for 15 minutes followed by surface cell staining with the appropriate antibodies. Next, cells were incubated with the FLICA reagent for 30 minutes at 37°C. After washing, cells were incubated in cold PBS with Sytox Orange (Thermo Fisher Scientific) for at least 20 minutes and acquired in the flow cytometer. For pSTAT5 quantification, cells were washed in cold PBS, fixed for 10 minutes in 1.6% formalin in cell culture RPMI, and fixed overnight at –20°C in 90% methanol. Next, cells were washed twice and stained for 45 minutes at room temperature with a dilution of 8:100 of Alexa Fluor 647 Mouse Anti-Stat5 (clone 47/Stat5 [pY694]) before a final wash and acquisition by flow cytometry.

CTL cytotoxic activity

Spleen cells from WT and cKO OT-I mice were differentiated to CTLs after red blood cell lysis in the presence of 0.5 μg/mL SIINFEKL and 100 U/mL rhIL-2 for 7 days (culture medium and IL-2 were replenished every other day). At day 7, CD8$^+$ T cells were isolated by negative selection. Spleen cells from C57BL/6 mice served as stimulating or target cells. CD8$^+$ T cells were pulsed (or not) with 1 μg/mL SIINFEKL for 1 hour at 37°C. For granzyme B production, CTLs were incubated overnight with pulsed spleen cells, and Brefeldin A (5 μg/mL) was added during the final 5 hours of culture. Then, cells were stained with the cytofix/cytoperm kit. To determine CTL degranulation, CD107a cell surface expression was assessed. To this end, CTLs were incubated for 5 hours with either control or pulsed cells in the presence of anti–mouse CD107a (1:250 dilution), Monesin (2 μM) and Brefeldin A. After 5 hours, cells were surface stained to identify OT-I (Vα2$^+$Vβ5$^+$) CD8$^+$ T cells. For the in vitro cytotoxicity assay, unpulsed and pulsed target cells were labeled with different concentrations of cell trace far red (CTFR): 0.1 μM and 1 μM, respectively. CTLs (effector cells) were incubated at different ratios with 75,000 target cells for 5 hours, and CD3$^-$CD4$^-$CD8$^-$ target cell death was measured by Sytox Orange staining.

Gene silencing

Specific shRNA sequences (Supplemental Table 4) were designed using the Broad Institute GPP Web Portal and cloned into LeGO-G

or LeGO-Cer. Lentiviral particles were generated in HEK293T/17 cells by cotransfecting the expression plasmid along with psPAX2 and pMD2.G packaging- and envelope-encoding plasmids. Purified T cells were activated in vitro as previously detailed. Next day, cells were infected with gene-specific (or control) shRNA-encoding lentiviruses in the presence of polybrene (3 μg/mL). Gene silencing was corroborated by qPCR in sorted cells.

Real-time PCR

Total RNA for real-time PCR was extracted and purified using TRIzol. Reverse transcription was performed in 1 μg of total using SCRIPT Reverse Transcriptase (Jena Bioscience), following the manufacturer's instructions, using oligo-dT primers. Real-time PCR was performed with SYBR Green (Thermo Fisher Scientific) labeling in a CFX96 Touch Real-Time PCR Detection System (Bio-Rad). PCR conditions were 95°C for 10 minutes, followed by 45 cycles of 95°C for 15 seconds and 60°C for 1 minute. mRNA expression was normalized against β-actin. Primers used in this study are listed in Supplemental Table 5.

Western blotting

Cells were lysed in RIPA buffer (15 μL of buffer per million cells) during 20 minutes on ice. Next, they were centrifuged for 10 minutes at 4°C (15,000*g*) and the supernatant was collected and frozen (–80°C). Cell lysates were thawed on ice and protein concentration was determined using Quick-start Bradford Dye (Bio-Rad). Normalized lysates were denatured by boiling in Laemmli buffer and separated in SDS-PAGE. Proteins were transferred to a PVDF membrane (Thermo Fisher Scientific) and detection was done using the indicated primary antibodies, followed by peroxidase-coupled secondary antibodies (Pierce). Proteins were visualized by chemiluminescence (Pierce ECL Western blotting substrate).

Production of lentiviral particles and cell transduction

HEK293T/17 cells were plated in 10-cm Petri dishes in full DMEM. When approximately 70% confluent, culture medium was replaced with Opti-MEM I (Gibco) and transfected with 10 μg shRNA-encoding plasmids or cDNA-encoding plasmids plus 3.5 μg MD2.G and 6.5 μg psPAX2 using Lipofectamine 2000 (Thermo Fisher Scientific). Twenty-four hours after transfection, culture medium was replaced with fresh full DMEM. Lentivirus-containing medium was harvested at 48 and 72 hours after transfection, concentrated using polyethylene glycol (MilliporeSigma), and stored at –80°C until use. Human T cells were isolated and activated as described before, and lentiviral particles were added at day 1 of in vitro activation in the presence of Polibrene (MilliporeSigma, 3 μg/mL). Efficiency of infection was evaluated using flow cytometry and was always between 40% and 75%.

Evaluation of FoxO1 nuclear translocation

MCF-7 cells were plated in 24-well plates in full DMEM. When they reached 70% confluence, they were transfected with a plasmid encoding a FoxO1-GFP fusion protein (38) plus pLVX-EF1α-IRES-mCherry (control) or pLVX-EF1α-*PPP2R2B*-IRES-mCherry. Twenty-four hours later, membrane-permeable Hoechst 33342 (Thermo Fisher Scientific, 100 ng/mL) was added and cells were imaged in an Eclipse TS100 inverted fluorescence microscope (Nikon). One hundred cotransfected cells were quantified per well. Each experiment was performed in triplicate.

Statistics

Statistical tests were calculated using Microsoft Excel and GraphPad Prism. The statistical tests and *P* values are indicated in the figures. In general, for comparison between 2 groups, 2-tailed paired or nonpaired Student's *t* test was used. The number of times each experiment was repeated is indicated in each figure. Data are presented as mean ± SD or SEM (indicated in each figure). *P* values less than 0.05 were considered statistically significant. Normal distributions were assumed and no specific method was used to determine whether the data met assumptions of the statistical approach used. No randomization and/or stratification method was applied.

Study approval

The study was approved by the Research and Ethics Committees of the INCMNSZ (IRE-1805). All participants signed informed consent forms. All experiments involving mice were done in accordance with the Guide for the Care and Use of Laboratory Animals. The Animal Care and Use Committees of the Instituto Nacional de Ciencias Médicas y Nutrición Salvador Zubirán (INCMNSZ; IRE-1805) and of the Beth Israel Deaconess Medical Center approved all the performed procedures.

Author contributions

NRR, IKMS, SAA, FR, and JCC conceptualized the study and designed the methodology. NRR, IKMS, JACS, HBGG, SAA, ASM, MEV, TN, DPRR, and JCC carried out the investigation. GCT and JAV contributed resources. JCC wrote the original draft. NRR, JACS, SAA, GCT, JAV, FR, and JCC reviewed and edited the manuscript. JAV, GCT, FR, and JCC acquired funding. FR and JCC provided supervision. The order of the co–first authors was determined by data contribution: NRR produced 56% and IKMS 44% of the data presented in the main figures.

Acknowledgments

We thank Michael Bevan and Mary Chase from the University of Washington for providing the ovalbumin-expressing *L. monocytogenes*. We thank Claudia González Espinoza (Cinvestav Sur) for sharing reagents. We thank Gloria Soldevila and Sandra Ortega from the Instituto de Investigaciones Biomédicas (IIB), Universidad Nacional Autónoma de México (UNAM), for providing CD45.1 mice. We thank Laura Bonifaz (Instituto Mexicano del Seguro Social) for sharing B16-OVA cells. We thank Rogelio Hernández-Pando and Jorge Barrios-Payán from the Pathology Department at the Instituto Nacional de Ciencias Médicas y Nutrición Salvador Zubirán (INCMNSZ) for sharing their BSL3 facility. We thank Misael Vega, Marysol Hernández, and Mariela Contreras-Escamilla (INCMNSZ), as well as Daniel Garzón, Marisela Hernández, and Georgina Díaz (IIB, UNAM) for their help handling our mouse colonies. We thank Araceli Martínez and Guadalupe Osornio for help procuring blood samples. We thank Patricia Espinoza and Cristina Campos for administrative assistance. NRR was the recipient of a Careers in Immunology American Association of Immunologists fellowship award and a Dirección General de Asuntos de Personal Académico–UNAM postdoctoral fellowship. This work was supported by grants from the NIH (National Institute of Arthritis and Musculoskeletal and Skin

Diseases, R21 AR063262 to JCC; National Institute of Allergy and Infectious Disease, R01 AI136924 to GCT), the Alliance for Lupus Research (244883 to JCC), and Consejo Nacional de Ciencia y Tecnología (IFC-2016-2047 to JCC; IFC-2015-549 to JAV; INFR-2015-01-253812, FOSISS-2016-39996, and CB-2017-34557 to FR).

Address correspondence to: José C. Crispín and Florencia Rosetti, Departamento de Inmunología y Reumatología, Instituto Nacional de Ciencias Médicas y Nutrición Salvador Zubirán, Vasco de Quiroga 15, Tlalpan, 14080, Mexico City, Mexico. Phone: 5255.5487.0900 ext. 2610; Email: carlos.crispina@incmnsz.mx (JCC); florencia.rosettis@incmnsz.mx (FR).

NRR's present address is: Medical Research Council, Laboratory of Molecular Biology, Cambridge, United Kingdom. SAA's present address is: Division of Rheumatology, University of Pennsylvania, Philadelphia, Pennsylvania, USA. MEV's present address is: Dirección de Investigación, Hospital General de México "Dr. Eduardo Liceaga", Mexico City, Mexico.

1. Shi Y. Serine/threonine phosphatases: mechanism through structure. *Cell*. 2009;139(3):468–484.
2. Arroyo JD, Hahn WC. Involvement of PP2A in viral and cellular transformation. *Oncogene*. 2005;24(52):7746–7755.
3. Sontag JM, Sontag E. Protein phosphatase 2A dysfunction in Alzheimer's disease. *Front Mol Neurosci*. 2014;7:16.
4. Katsiari CG, Kyttaris VC, Juang YT, Tsokos GC. Protein phosphatase 2A is a negative regulator of IL-2 production in patients with systemic lupus erythematosus. *J Clin Invest*. 2005;115(11):3193–3204.
5. Janssens V, Longin S, Goris J. PP2A holoenzyme assembly: in cauda venenum (the sting is in the tail). *Trends Biochem Sci*. 2008;33(3):113–121.
6. Crispín JC, et al. Cutting edge: protein phosphatase 2A confers susceptibility to autoimmune disease through an IL-17-dependent mechanism. *J Immunol*. 2012;188(8):3567–3571.
7. Apostolidis SA, et al. Phosphatase PP2A is requisite for the function of regulatory T cells. *Nat Immunol*. 2016;17(5):556–564.
8. Holmes SE, et al. Expansion of a novel CAG trinucleotide repeat in the 5' region of PPP2R2B is associated with SCA12. *Nat Genet*. 1999;23(4):391–392.
9. Lin CH, et al. The CAG repeat in SCA12 functions as a cis element to up-regulate PPP2R2B expression. *Hum Genet*. 2010;128(2):205–212.
10. Dagda RK, et al. The spinocerebellar ataxia 12 gene product and protein phosphatase 2A regulatory subunit Bbeta2 antagonizes neuronal survival by promoting mitochondrial fission. *J Biol Chem*. 2008;283(52):36241–36248.
11. Cohen RL, Margolis RL. Spinocerebellar ataxia type 12: clues to pathogenesis. *Curr Opin Neurol*. 2016;29(6):735–742.
12. Tan J, et al. B55β-associated PP2A complex controls PDK1-directed myc signaling and modulates rapamycin sensitivity in colorectal cancer. *Cancer Cell*. 2010;18(5):459–471.
13. Majchrzak-Celińska A, Słocińska M, Barciszewska AM, Nowak S, Baer-Dubowska W. Wnt pathway antagonists, SFRP1, SFRP2, SOX17, and PPP2R2B, are methylated in gliomas and SFRP1 methylation predicts shorter survival. *J Appl Genet*. 2016;57(2):189–197.
14. Yang Y, et al. Identification of differentially expressed genes in the development of osteosarcoma using RNA-seq. *Oncotarget*. 2016;7(52):87194–87205.
15. Crispín JC, Apostolidis SA, Finnell MI, Tsokos GC. Induction of PP2A Bβ, a regulator of IL-2 deprivation-induced T-cell apoptosis, is deficient in systemic lupus erythematosus. *Proc Natl Acad Sci USA*. 2011;108(30):12443–12448.
16. Madera-Salcedo IK, et al. PPP2R2B hypermethylation causes acquired apoptosis deficiency in systemic autoimmune diseases. *JCI Insight*. 2019;5:126457.
17. Marrack P, Scott-Browne J, MacLeod MK. Terminating the immune response. *Immunol Rev*. 2010;236:5–10.
18. Snow AL, Pandiyan P, Zheng L, Krummey SM, Lenardo MJ. The power and the promise of restimulation-induced cell death in human immune diseases. *Immunol Rev*. 2010;236:68–82.
19. Hildeman DA, et al. Activated T cell death in vivo mediated by proapoptotic bcl-2 family member bim. *Immunity*. 2002;16(6):759–767.
20. Bouillet P, O'Reilly LA. CD95, BIM and T cell homeostasis. *Nat Rev Immunol*. 2009;9(7):514–519.
21. Snow AL, et al. Restimulation-induced apoptosis of T cells is impaired in patients with X-linked lymphoproliferative disease caused by SAP deficiency. *J Clin Invest*. 2009;119(10):2976–2989.
22. Chinen T, et al. An essential role for the IL-2 receptor in T_{reg} cell function. *Nat Immunol*. 2016;17(11):1322–1333.
23. Saxton RA, Sabatini DM. mTOR signaling in growth, metabolism, and disease. *Cell*. 2017;168(6):960–976.
24. Wlodarchak N, Xing Y. PP2A as a master regulator of the cell cycle. *Crit Rev Biochem Mol Biol*. 2016;51(3):162–184.
25. Kim AH, Khursigara G, Sun X, Franke TF, Chao MV. Akt phosphorylates and negatively regulates apoptosis signal-regulating kinase 1. *Mol Cell Biol*. 2001;21(3):893–901.
26. Stambolic V, et al. Negative regulation of PKB/Akt-dependent cell survival by the tumor suppressor PTEN. *Cell*. 1998;95(1):29–39.
27. Datta SR, et al. Akt phosphorylation of BAD couples survival signals to the cell-intrinsic death machinery. *Cell*. 1997;91(2):231–241.
28. Stephens L, et al. Protein kinase B kinases that mediate phosphatidylinositol 3,4,5-trisphosphate-dependent activation of protein kinase B. *Science*. 1998;279(5351):710–714.
29. Sarbassov DD, Guertin DA, Ali SM, Sabatini DM. Phosphorylation and regulation of Akt/PKB by the rictor-mTOR complex. *Science*. 2005;307(5712):1098–1101.
30. Brunet A, et al. Akt promotes cell survival by phosphorylating and inhibiting a Forkhead transcription factor. *Cell*. 1999;96(6):857–868.
31. Sato S, Fujita N, Tsuruo T. Modulation of Akt kinase activity by binding to Hsp90. *Proc Natl Acad Sci USA*. 2000;97(20):10832–10837.
32. Araki K, et al. Translation is actively regulated during the differentiation of $CD8^+$ effector T cells. *Nat Immunol*. 2017;18(9):1046–1057.
33. Toker A, Marmiroli S. Signaling specificity in the Akt pathway in biology and disease. *Adv Biol Regul*. 2014;55:28–38.
34. Zhang X, Tang N, Hadden TJ, Rishi AK. Akt, FoxO and regulation of apoptosis. *Biochim Biophys Acta*. 2011;1813(11):1978–1986.
35. Kops GJ, de Ruiter ND, De Vries-Smits AM, Powell DR, Bos JL, Burgering BM. Direct control of the Forkhead transcription factor AFX by protein kinase B. *Nature*. 1999;398(6728):630–634.
36. Nakae J, Park BC, Accili D. Insulin stimulates phosphorylation of the forkhead transcription factor FKHR on serine 253 through a Wortmannin-sensitive pathway. *J Biol Chem*. 1999;274(23):15982–15985.
37. Singh A, et al. Protein phosphatase 2A reactivates FOXO3a through a dynamic interplay with 14-3-3 and AKT. *Mol Biol Cell*. 2010;21(6):1140–1152.
38. Nakamura N, Ramaswamy S, Vazquez F, Signoretti S, Loda M, Sellers WR. Forkhead transcription factors are critical effectors of cell death and cell cycle arrest downstream of PTEN. *Mol Cell Biol*. 2000;20(23):8969–8982.
39. van der Vos KE, Coffer PJ. The extending network of FOXO transcriptional target genes. *Antioxid Redox Signal*. 2011;14(4):579–592.
40. Eijkelenboom A, et al. Genome-wide analysis of FOXO3 mediated transcription regulation through RNA polymerase II profiling. *Mol Syst Biol*. 2013;9:638.
41. Huang DC, Strasser A. BH3-only proteins-essential initiators of apoptotic cell death. *Cell*. 2000;103(6):839–842.
42. Imaizumi K, Tsuda M, Imai Y, Wanaka A, Takagi T, Tohyama M. Molecular cloning of a novel polypeptide, DP5, induced during programmed neuronal death. *J Biol Chem*. 1997;272(30):18842–18848.
43. Chen L, et al. SYK inhibition modulates distinct PI3K/AKT- dependent survival pathways and cholesterol biosynthesis in diffuse large B cell lymphomas. *Cancer Cell*. 2013;23(6):826–838.
44. Szydlowski M, et al. FOXO1 activation is an effector of SYK and AKT inhibition in tonic BCR signal-dependent diffuse large B-cell lymphomas. *Blood*. 2016;127(6):739–748.
45. Ross SH, Cantrell DA. Signaling and function of

interleukin-2 in T lymphocytes. *Annu Rev Immunol*. 2018;36:411–433.
46. Vella AT, Dow S, Potter TA, Kappler J, Marrack P. Cytokine-induced survival of activated T cells in vitro and in vivo. *Proc Natl Acad Sci USA*. 1998;95(7):3810–3815.
47. Zhao YY, et al. Effects of an oral allosteric AKT inhibitor (MK-2206) on human nasopharyngeal cancer in vitro and in vivo. *Drug Des Devel Ther*. 2014;8:1827–1837.
48. Pellegrini M, Belz G, Bouillet P, Strasser A. Shutdown of an acute T cell immune response to viral infection is mediated by the proapoptotic Bcl-2 homology 3-only protein Bim. *Proc Natl Acad Sci USA*. 2003;100(24):14175–14180.
49. Häcker G, Bauer A, Villunger A. Apoptosis in activated T cells: what are the triggers, and what the signal transducers? *Cell Cycle*. 2006;5(21):2421–2424.
50. Manning BD, Toker A. AKT/PKB signaling: navigating the network. *Cell*. 2017;169(3):381–405.
51. Srinivasan L, et al. PI3 kinase signals BCR-dependent mature B cell survival. *Cell*. 2009;139(3):573–586.
52. Na SY, et al. Constitutively active protein kinase B enhances Lck and Erk activities and influences thymocyte selection and activation. *J Immunol*. 2003;171(3):1285–1296.
53. Rathmell JC, Elstrom RL, Cinalli RM, Thompson CB. Activated Akt promotes increased resting T cell size, CD28-independent T cell growth, and development of autoimmunity and lymphoma. *Eur J Immunol*. 2003;33(8):2223–2232.
54. Juntilla MM, Wofford JA, Birnbaum MJ, Rathmell JC, Koretzky GA. Akt1 and Akt2 are required for alphabeta thymocyte survival and differentiation. *Proc Natl Acad Sci USA*. 2007;104(29):12105–12110.
55. Mao C, et al. Unequal contribution of Akt isoforms in the double-negative to double-positive thymocyte transition. *J Immunol*. 2007;178(9):5443–5453.
56. Nagata S, Tanaka M. Programmed cell death and the immune system. *Nat Rev Immunol*. 2017;17(5):333–340.
57. Happo L, Strasser A, Cory S. BH3-only proteins in apoptosis at a glance. *J Cell Sci*. 2012;125(Pt 5):1081–1087.
58. Jeffers JR, et al. Puma is an essential mediator of p53-dependent and -independent apoptotic pathways. *Cancer Cell*. 2003;4(4):321–328.
59. Villunger A, et al. p53- and drug-induced apoptotic responses mediated by BH3-only proteins puma and noxa. *Science*. 2003;302(5647):1036–1038.
60. Sanz C, Benito A, Inohara N, Ekhterae D, Nunez G, Fernandez-Luna JL. Specific and rapid induction of the proapoptotic protein Hrk after growth factor withdrawal in hematopoietic progenitor cells. *Blood*. 2000;95(9):2742–2747.
61. Coultas L, et al. Hrk/DP5 contributes to the apoptosis of select neuronal populations but is dispensable for haematopoietic cell apoptosis. *J Cell Sci*. 2007;120(Pt 12):2044–2052.
62. Oda E, et al. Noxa, a BH3-only member of the Bcl-2 family and candidate mediator of p53-induced apoptosis. *Science*. 2000;288(5468):1053–1058.
63. Ranger AM, et al. Bad-deficient mice develop diffuse large B cell lymphoma. *Proc Natl Acad Sci USA*. 2003;100(16):9324–9329.
64. Gupta S, Gollapudi S. Effector memory CD8+ T cells are resistant to apoptosis. *Ann N Y Acad Sci*. 2007;1109:145–150.
65. Larsen SE, Voss K, Laing ED, Snow AL. Differential cytokine withdrawal-induced death sensitivity of effector T cells derived from distinct human $CD8^+$ memory subsets. *Cell Death Discov*. 2017;3:17031.
66. Redeker A, Arens R. Improving adoptive T cell therapy: the particular role of T cell costimulation, cytokines, and post-transfer vaccination. *Front Immunol*. 2016;7:345.
67. Weber K, Bartsch U, Stocking C, Fehse B. A multicolor panel of novel lentiviral "gene ontology" (LeGO) vectors for functional gene analysis. *Mol Ther*. 2008;16(4):698–706.
68. Zehn D, Lee SY, Bevan MJ. Complete but curtailed T-cell response to very low-affinity antigen. *Nature*. 2009;458(7235):211–214.
69. Pope C, et al. Organ-specific regulation of the CD8 T cell response to Listeria monocytogenes infection. *J Immunol*. 2001;166(5):3402–3409.